AD-A176 808 FRACTURE AND HARDNESS OF SEMICONDUCTOR ALLOYS(U) SRI INTERNATIONAL MENLO PARK CA A SHER ET AL 05 NOV 86 AFOSR-TR-87-0160 F49620-85-K-0023 1/1

UNCLASSIFIED F/G 20/12 NL

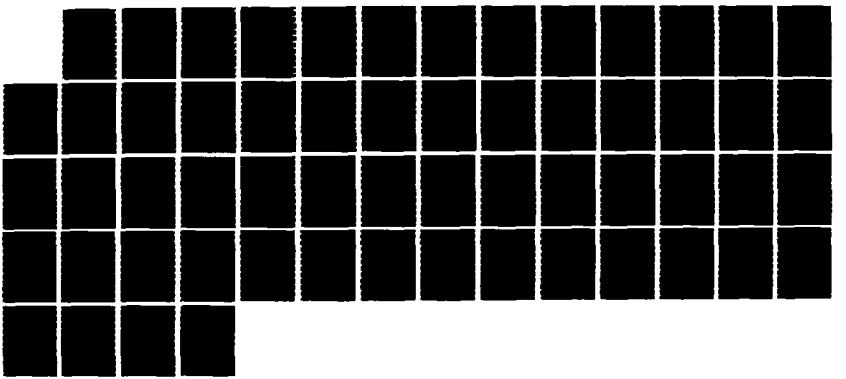

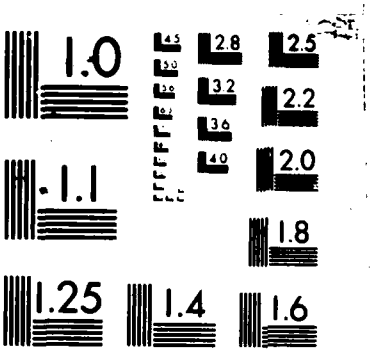

AFOSR-TR- 87-0160

FRACTURE AND HARDNESS OF SEMICONDUCTOR ALLOYS

Annual Technical Report

November 1986

By: A. Sher, M. van Schilfgaarde, A.-B. Chen, and M. Berding

Prepared for:

United States Air Force
Air Force Systems Command
Directorate of Electronic and Materials Sciences
Building 410
Bolling Air Force Base, D.C. 20332-6448

Attn: Capt. Kevin J. Malloy

Contract F49620-85-K-0023

SRI Project 1142

SRI International
333 Ravenswood Avenue
Menlo Park, California 94025-3493
(415) 326-6200
Telex: 334486

UNCLASSIFIED
SECURITY CLASSIFICATION OF THIS PAGE

REPORT DOCUMENTATION PAGE

1a. REPORT SECURITY CLASSIFICATION Unclassified	1b. RESTRICTIVE MARKINGS AD-A176 820
2a. SECURITY CLASSIFICATION AUTHORITY	3. DISTRIBUTION/AVAILABILITY OF REPORT Approved for public release;
2b. DECLASSIFICATION/DOWNGRADING SCHEDULE	distribution unlimited.
4. PERFORMING ORGANIZATION REPORT NUMBER(S)	5. MONITORING ORGANIZATION REPORT NUMBER(S) AFOSR-TR- 87-0160
6a. NAME OF PERFORMING ORGANIZATION SRI International 6b. OFFICE SYMBOL (if applicable)	7a. NAME OF MONITORING ORGANIZATION ~~USAF, AFSC~~ AFOSR Directorate of Electronic and Material Sciences
6c. ADDRESS (City, State, and ZIP Code) 333 Ravenswood Avenue Menlo Park, California 94025-3493	7b. ADDRESS (City, State, and ZIP Code) Building 41 Bolling AFB, D.C. 20332-6448
8a. NAME OF FUNDING/SPONSORING ORGANIZATION USAF/AFOSR AFOSR 8b. OFFICE SYMBOL (if applicable) NE	9. PROCUREMENT INSTRUMENT IDENTIFICATION NUMBER F49620-85-K-0023
8c. ADDRESS (City, State, and ZIP Code) Directorate of Electronic and Material Sciences AFOSR/NE; Building 41 Bolling AFB, D.C. 20332-6448	10. SOURCE OF FUNDING NUMBERS PROGRAM ELEMENT NO. 61102F; PROJECT NO. 2306; TASK NO. B1; WORK UNIT ACCESSION NO.

11. TITLE (Include Security Classification)

Fracture and Hardness of Semiconductor Alloys

12. PERSONAL AUTHOR(S)

A. Sher, M. van Schilfgaarde, A.-B. Chen, and M. Berding

13a. TYPE OF REPORT	13b. TIME COVERED	14. DATE OF REPORT (Year, Month, Day)	15. PAGE COUNT
Annual Technical	FROM 1 Sep 85 TO 31 Aug 86	1986 November 5	57

16. SUPPLEMENTARY NOTATION

17. COSATI CODES			18. SUBJECT TERMS (Continue on reverse if necessary and identify by block number)
FIELD	GROUP	SUB-GROUP	semiconductor alloys, fracture, hardness, anisotropic hardness, vacancy, bond energies, elastic coefficients

19. ABSTRACT (Continue on reverse if necessary and identify by block number)

We demonstrate that the atomic distribution of constituents in semiconductor alloys is never random. There are always interactions causing correlations; the degree and nature of the correlations depend on which interactions dominate and on the growth condition. We have identified most of the interactions that are expected to cause correlations: electron/electron Coulomb-interactions, and chemical and strain energies. We have developed a method to calculate accurate bond lengths, bond energies, and elastic coefficients for semiconductor compounds. Work has begun to incorporate anisotropicity into the theory of hardness. A calculation of the vacancy formation energies in compounds and dilute alloys has been completed; it will be generalized to concentrated alloys in the future.

20. DISTRIBUTION/AVAILABILITY OF ABSTRACT	21. ABSTRACT SECURITY CLASSIFICATION
☐ UNCLASSIFIED/UNLIMITED ☐ SAME AS RPT. ☐ DTIC USERS	Unclassified
22a. NAME OF RESPONSIBLE INDIVIDUAL KEVIN Mackay	22b. TELEPHONE (Include Area Code) 767-4931
	22c. OFFICE SYMBOL NE

DD FORM 1473, 84 MAR 83 APR edition may be used until exhausted. All other editions are obsolete.

SECURITY CLASSIFICATION OF THIS PAGE
UNCLASSIFIED

SRI International

FRACTURE AND HARDNESS OF SEMICONDUCTOR ALLOYS

Annual Technical Report

November 1986

By: A. Sher, M. van Schilfgaarde, A.-B. Chen, and M. Berding

Prepared for:

United States Air Force
Air Force Systems Command
Directorate of Electronic and Materials Sciences
Building 410
Bolling Air Force Base, D.C. 20332-6448

Attn: Capt. Kevin J. Malloy

Contract F49620-85-K-0023

SRI Project 1142

Approved:

Ivor Brodie, Director
Physical Electronics Laboratory

W.F. Greenman, Vice President
Advanced Technology Division

SRI International®

CONTENTS

ILLUSTRATIONS

TABLES

I INTRODUCTION

The objectives of the research reported here, as outlined in the Statement of Work in SRI's Proposal for Research EDU 85-79 (for a three-year effort), are the following:

- Calculate the angular dependence of the hardness.
- Determine the transient response of the hardness.
- Improve the accuracy of the strain coefficient calculations for pure semiconductors.
- Calculate the alloy composition variation of the strain coefficients.
- Develop an extension in terms of microscopic quantities of the Griffith crack propagation theory.
- Deduce a theory of crack initiation.
- Devise strategies for improving the fracture characteristics of semiconductors.

This report covers our accomplishments in the first year of the three-year effort.

In this period, we have concentrated much of our efforts on our new statistical theory of order/disorder transitions. The work has reached a plateau that warrants publication and a long paper is in preparation. The manuscript will be done in about a week, and the finished document will be completed and sent to AFOSR within a month; the major conclusions are presented in Section II.

We have discovered that the electron/electron Coulomb interactions, as modified by long-ranged Madelung sums, represent a new and major contribution to the mixing enthalpy and more generally to atomic correlations in alloys. This term is driven by polarity mismatches, rather than the bond-length mismatches traditionally thought to be responsible for mixing enthalpies. The major results of this aspect of the work are in Section III.

We have also found a method to calculate accurately the bond lengths, bond energies, and elastic coefficients of all the semiconductor compounds. The results are summarized in Section IV. While no detailed calculations are completed, we also have devised a way to extend these calculations to alloys. This extension is also discussed in Section IV.

The present status of our work on the angular dependence of the hardness is presented in Section V. Significant progress has been made on the vacancy-formation-energy problem, both for pure compounds and alloys, and they are outlined in Section VI. This is an essential ingredient in the understanding of a number of dislocation-related phenomena.

Appendices A and B to this report are reprints of publications in the technical literature that were written with support from this contract. Appendix C is the chronological list of publications under this contract, while Appendix D lists the professional personnel who have contributed to this work, and Appendix E describes the interactions.

II CORRELATIONS IN SEMICONDUCTOR ALLOYS

We have demonstrated (Chen and Sher, 1985a, 1985b; Sher, Chen, and van Schilfgaarde, 1986) that the atomic distribution of constituents in semiconductor alloys is never truly random. There are always interactions causing correlations; the degree and nature of the correlations depend on which interactions dominate and on the growth conditions. While we have identified most of the interactions that are expected to cause correlations, not all of them have been treated completely to date. Therefore, while some details remain unclear, the principal effects can now be appreciated in broad terms, and we shall attempt to identify them in the following discussion.

In the formalism reported here, we start by focusing on small clusters of atoms that are called *microclusters*. Once the microcluster size is selected, the total energy of the solid is expressed as a sum of cluster energies, and the number of configurations of the solid corresponding to a given total energy is calculated. Some approximations in the microcluster energy calculations and microcluster/microcluster interactions are neglected, but once these approximations are made, there is no appreciable additional inaccuracy introduced in the statistical mechanics arguments leading to microcluster population distributions. The accuracy of the final result for a given physical property (e.g. critical order/disorder transition temperature) differs for different properties, but in general becomes progressively better the larger the cluster size used. Two atom clusters are found to give most trends properly, but differ in detail from the answers found for the five-atom, sixteen-bond clusters that are the basis for most of the numerical results presented in this report. We have not attempted to extend the numerical results for larger clusters.

We have demonstrated that for an n-atom microcluster in state j, represented schematically as $A_{n-n_j(B)}B_{n_j(B)}$, corresponding to a given number $n_j(B)$ of B atoms if the degeneracy $g_j = \binom{n}{n_j(B)}$ of a given energy state ε_j is not split, and if ε_j depends linearly on $n_j(B)$, then the average population distribution $\bar{x}_j$ is always that of a random alloy x_j^0. Therefore, only interactions that split the degeneracy or cause a nonlinear variation of ε_j on $n_j(B)$ drive correlations. To be precise (as can be seen from the detailed analysis), the energies $\varepsilon_j - n_j(B)\mu(B)$, where $\mu(B)$ is the B atom chemical potential in the grand partition function formalism, are responsible for populations of state j.

We have identified three mechanisms that cause appropriate nonlinear variations of ε_j:

- A type caused by strains resulting from bond-length mismatches between the constituents.
- *Chemical interactions*, caused by potential differences between the constituents that are responsible for charge shifts among the atoms, and in tight-binding terminology the ionic, covalent, and metallization contributions to bond energies.
- A type arising from the electron/electron Coulomb interactions as modified by long-ranged Madelung sums (van Schilfgaarde, Chen, and Sher, 1986).

As a rule, the bond-length mismatch terms dominate, but the other terms can introduce substantial corrections and in the exceptional cases (where there is a near-bond-length match) are all that remains. Until recently, it was thought that cluster energies were nearly independent of composition (Guggenheim, 1952). In consequence, if the average of the AA and BB interaction energies exceeded the AB energy, then compound formation was thought to be favored; while in the opposite case, spinodal decomposition was favored. The entropy terms always favor the intermediate random distribution.

We now know that this picture is flawed and that the cluster excess energies are in fact highly composition-dependent. In the strain terms, the cluster whose volume most closely matches the average volume per cluster for the alloy will have the lowest energy. As a consequence, certain alloy compositions (e.g. x = 0.25, 0.5, 0.75, where simple stoichiometric compounds with long-range order could exist) have comparatively low excess-free energies. This means that it is possible in principle to have a positive mixing entropy parameter defined by $\Omega \equiv -\Delta F/[x(1-x)]$ and still have compound formation favored for some special compositions x. However, this does not happen as a general rule. For example, in Figure 1(a) the excess enthalpy ΔE has no sharp feature at the special concentrations, even for material grown at room temperature. The shape of the corresponding free energy ΔF in Figure 1(b) is characteristic of a material that undergoes normal spinodal decomposition. Figure 2(a) exhibits the excess energy per microcluster ε_j variation with composition for each of the five-atom (16-bond) cluster types. Figures 2(b) and 3(a) display ε_j, and the corresponding excess free energies ΔF for a stiff-lattice case of $Ga_{1-x}In_xAs$, in which it has been assumed that the twelve outer bonds of the cluster are attached to C-type atoms that are fixed at lattice spacings corresponding to Vegard's rule. Even in this stiff-lattice case, normal spinodal decomposition is the rule. It is not until we also set the angular distortion elastic constant β in the Valence Force Field model to zero that the excess free energy curve for GaInAs in Figure 3(b) has a shape that corresponds to decomposition into an ordered compound and a random alloy. We have resisted the temptation to present phase diagrams (critical temperature versus composition) in this report because they will be modified substantially by the Coulomb interactions that are not yet incorporated completely into the formalism.

The chemical interactions modify this picture only slightly: They tend to cause a slight asymmetry in the excess enthalpy variation with x about x = 0.5 and to shift the overall curves. For $Ga_{1-x}In_xAs$, the asymmetry causes the features on the low-x side to have higher energies than the corresponding ones on the high-x side. We have demonstrated that the absolute shifts of the chemical excess energies are positive for the anion-substituted alloys and negative for the cation-substituted alloys (Chen and Sher, 1985b). Hence, for the same lattice constant mismatch, a cation-substituted alloy will have a smaller mixing enthalpy than an anion-substituted alloy.

The configuration-dependent electron/electron Coulomb interactions (van Schilfgaarde, Chen, and Sher, 1986) are not included in the results reported here. These interactions make contributions comparable to those driven by the bond-length differences discussed previously and, therefore, will modify the numerical results significantly. These terms are driven by polarity differences between the alloy constituents in contradistinction to the customary bond-length difference. The essential feature of Coulomb interactions is the configuration-dependence of spatial charge fluctuations. Because the Coulomb energy is nonlinear in the charge density, fluctuations always increase the energy. This can be partially compensated by

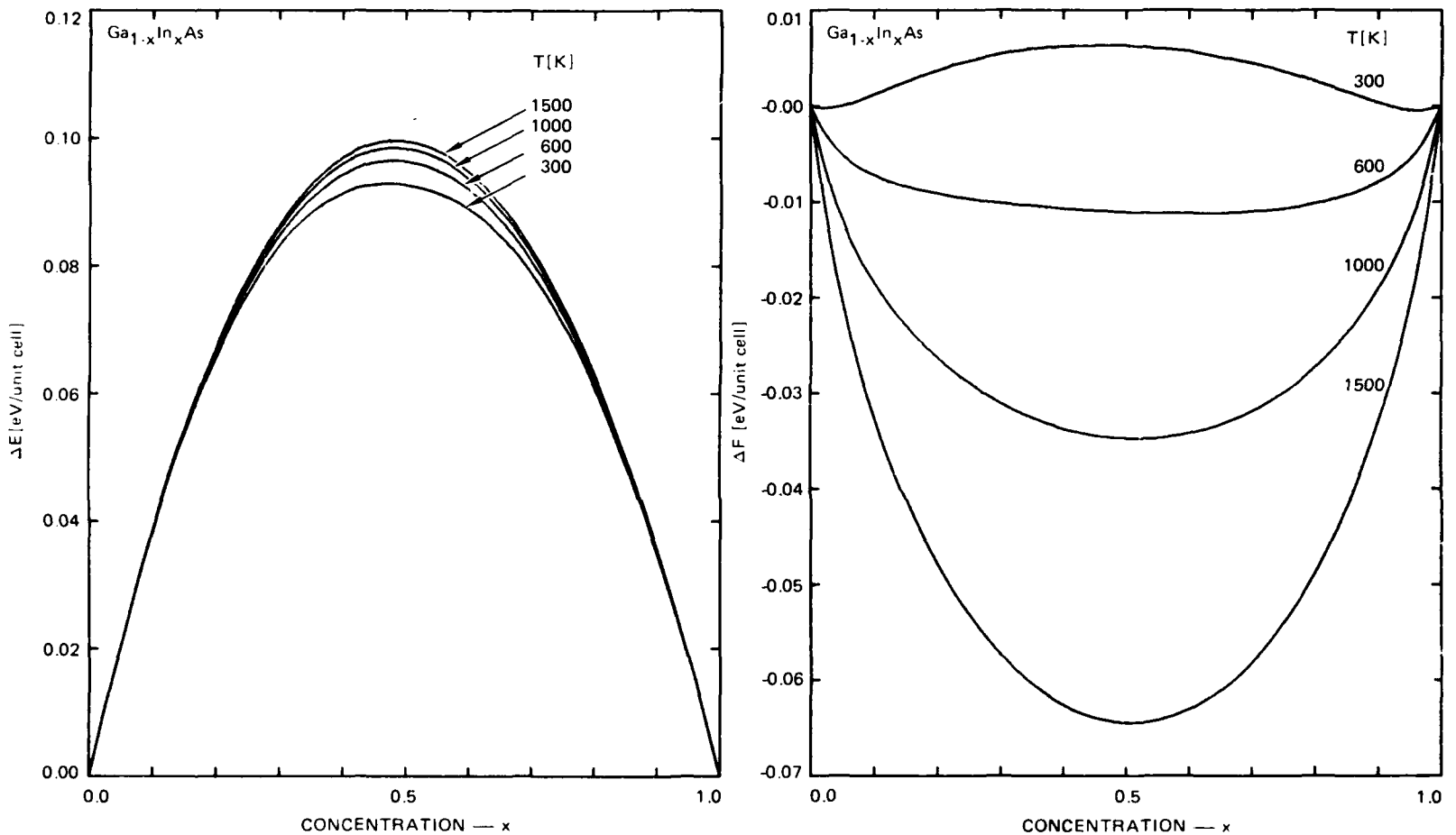

FIGURE 1 MIXING ENTHALPY AND FREE ENERGY PER UNIT CELL (FOUR BONDS) AS A FUNCTION OF THE CONCENTRATION x FOR FOUR GROWTH TEMPERATURES

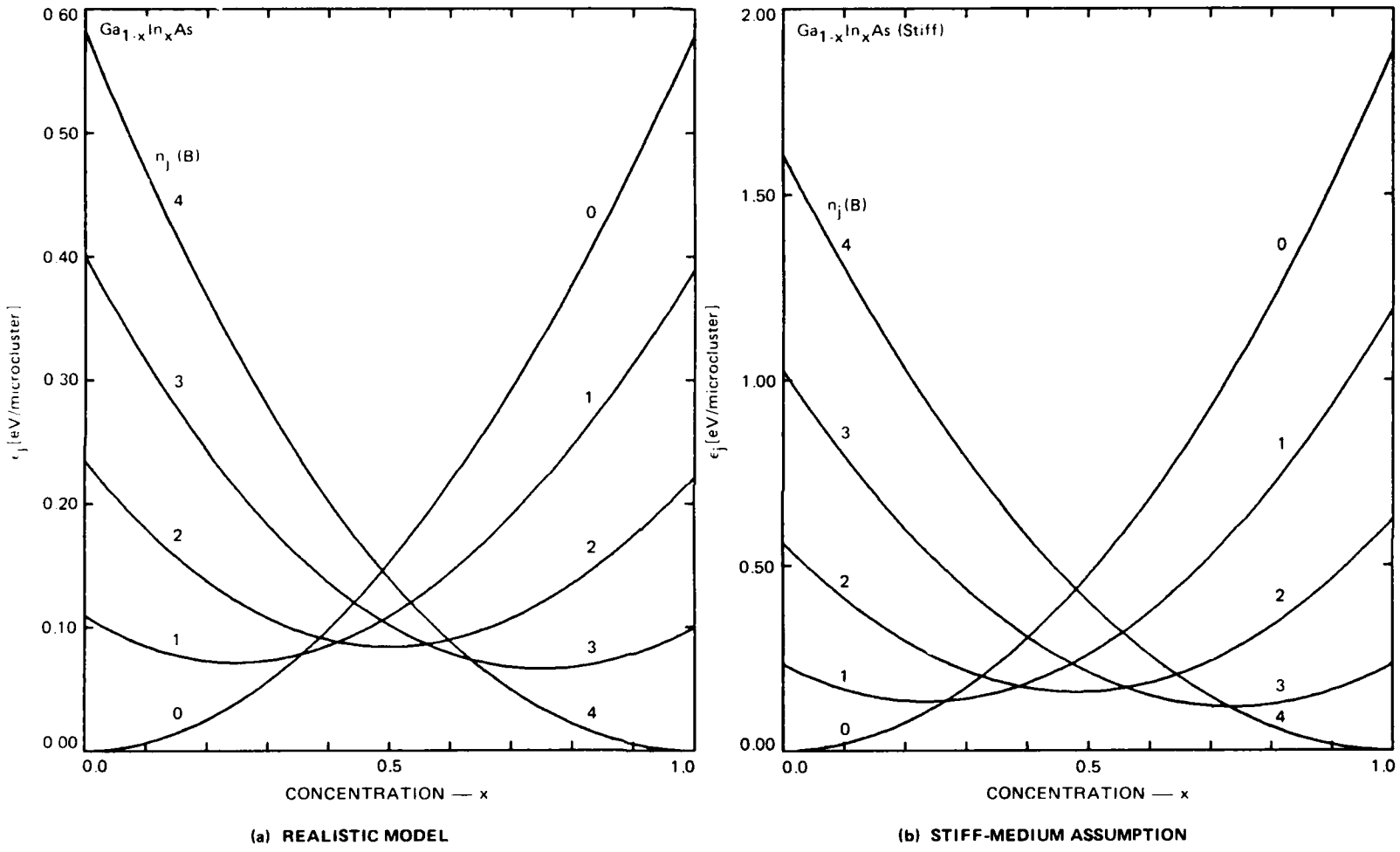

FIGURE 2 EXCESS ENERGY PER MICROCLUSTER FOR THE DIFFERENT CLUSTERS AS A FUNCTION OF CONCENTRATION x

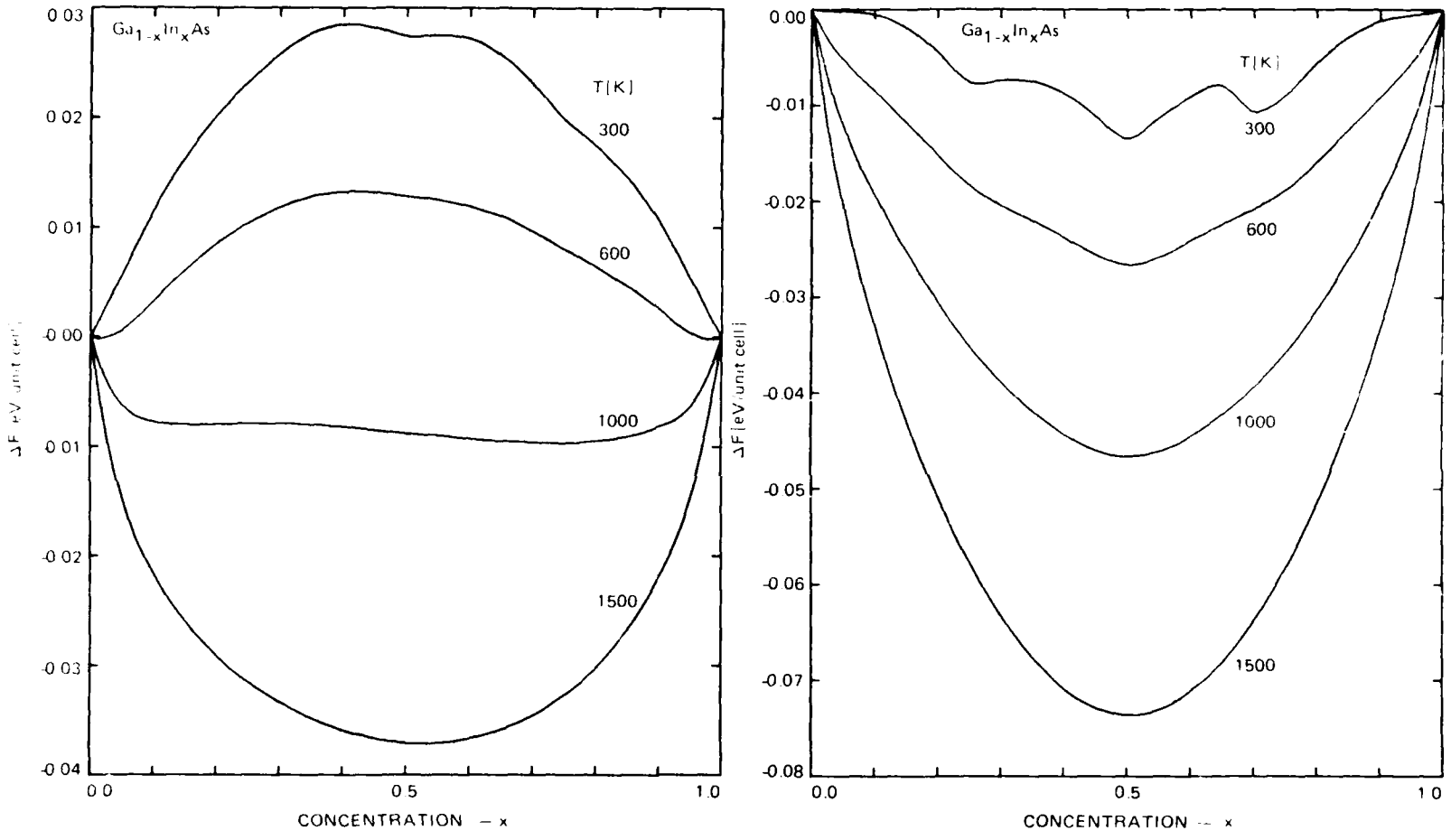

(a) NORMAL VALUE FOR β

(b) $\beta = 0$

FIGURE 3 FREE ENERGY PER UNIT CELL AS A FUNCTION OF CONCENTRATION x FOR FOUR GROWTH TEMPERATURES UNDER THE ASSUMPTION OF A STIFF MEDIUM

the long-range Madelung energy originating in a coherent sum of alternating charges. Configurations that minimize the combined effect are of lowest energy. The random configuration is always of higher energy, mainly because of the weakening of the Madelung energy. Therefore, both ordered compounds and spinodal decomposition are favored by this interaction relative to random alloys. We have demonstrated that in the bond-length-matched $Ga_{1-x}Al_xAs$ alloy, the ordering observed by Kuan, et al. (1985) can be explained by these electron/electron Coulomb terms.

Others (e.g. Czyzyk et al. 1986; Srinivastava, Martins, and Zunger, 1985) have calculated the concentration variation of microcluster energies ε_j by treating the various types of clusters as units of different periodic structures. These workers allow the central cation in each $A_{4-j}B_jC$ (j = 0,1,2,3,4) microcluster to relax into its minimum-energy configuration and then compute the energy of the cluster $\varepsilon_j(v)$ as a function of cluster volume v. They then assign cluster energies at each composition x by identifying the v to be that of the average lattice, following Vegard's rule. This procedure leads to negative cluster energies for the compositions where the cluster volume just fits the average alloy volume per cluster, so these special clusters experience no strain. In the plot of ε_j versus x in Figure 2(a), this would cause the A(3)B(1)C, A(2)B(2)C, A(1)B(3)C cluster energies to be negative for x = 0.25, 0.5, and 0.75, respectively. In addition, the constraint that each type of cluster has the same volume at a give concentration accentuates the differences between cluster energies relative to those we calculate and resemble the stiff lattice case in Figure 2(b). In our procedure, each cluster is attached to an effective alloy medium and allowed to relax to its minimum energy configuration. The effect of constraining the volume can be seen by comparing Figures 2(a) and 2(b). Thus, there are two major differences between our ε_j versus x curves and those of other groups. Even for cases with a bond-length mismatch, some of their ε_j values are negative for a collection of special concentrations corresponding to possible stoichiometric compounds for which the periodic lattice can fit together without appreciable strain. Furthermore, their ε_j values vary much more steeply with x reaching somewhat larger values and having a much larger overall excursion, because the various cluster volumes are each forced to equal the average lattice volume. This causes their free energy versus composition curves at a given temperature to have a much sharper structure than ours with three deep minima at x = 0.25, 0.5, and 0.75, similar to the results in Figure 3 (Guggenheim, 1952; Kuan et al., 1985), which we could generate only in a quite unphysical circumstance.

There is merit in both approaches. We suspect that their results are correct, but only in a very narrow composition range where the periodic structures exist and near the critical order/disorder transition temperature. The models reported to date assign to a microcluster only the local strain energy. However, there is also a long-range strain field produced in the surrounding medium by a cluster that does not fit exactly into the lattice. If there are many misfitting clusters, then the long-range strain fields from each add incoherently, and the net results is to produce the average lattice spacing, but no additional nonlocal energy need by counted toward each cluster. However, when the misfit cluster density is small, then the incoherence is incomplete and the long-range strain fields are likely to be important. Thus, starting from a perfectly ordered compound, e.g. ABC_2, the first small deviation in the composition from the ideal stoichiometry will introduce large (local and long-range) strain fields, which will cause the composition variation of the free energy around these special points to be even more rapid than anyone has yet calculated. Accordingly, the net result is expected to be low-temperature excess-free-energy curves that resemble those in Figure 1(b), but with sharp

negative spikes superimposed at the special compositions. This conjecture remains to be confirmed by calculation and experiment.

The other major class of phenomena that can introduce correlations are those that split the degeneracy of the clusters. The easiest ones to picture are coherent strains produced by a uniform externally applied stress. This can happen, for example, when an epitaxial layer of an alloy is grown on a lattice-mismatched substrate. Then, for example, for a stress in the <110> direction, a four-atom $n_j(B) = 2$ cluster will have different energies if the two B atoms or two A atoms have positive displacement components parallel to the <110> direction. When the stress is large enough to drive the energy of the preferred orientation down well below those of other clusters, then it is possible for compounds with long-range order to have low free energies. This phenomenon has recently been observed in the growth of $Ge_{0.5}Si_{0.5}$ on a silicon substrate, where an ordered compound, rather than a random alloy, was found (Bevk et al, 1986). Stresses produced by temperature gradients behind a growth front can cause similar effects. In this discussion, we have recognized the potential importance of applied stresses and temperature gradients in driving microcluster population distributions. However, a comprehensive quantitative theory must still be formulated.

We have discussed the possibility of spinodal decomposition into domains. A given domain can be nearly a random alloy surrounded by other domains with differing compositions or ordered compounds depending on the constituent materials, the concentration, and growth conditions. However, there remains the question of how the domains fit together and their relative size. We cannot offer complete answers to these questions, but we can identify many phenomena that influence the outcome. The thermodynamics discussed here tell us about the compositions and structure of the favored domains. Clearly, if there is no inhibition to atom motion or annealing times are *sufficiently long* for equilibrium to be reached, the system will separate into two domains, one of each of the favored types, and the relative amount of each type will be given by the composition-lever rule applied to the free-energy curve. However, if there are constraints on the distance atoms can travel, then there may be other local-free-energy minima determined by a competition between the statistical effects discussed previously and long-range strains produced as the alloy forms a domain structure. Because the different types of domains have different lattice constants when space in some regular array is filled with them, they will exert stresses on one another. The preferred configuration will be one that minimizes the net free energy, now including the extra mechanical domain/domain interactions. The calculation by Muller (1984), in which he demonstrates that the fluctuations in the populations of clusters inherent in a random alloy are suppressed by strain fields in lattice mismatched systems, is a precursor to this kind of theory. A regular array of domains of ordered compounds surrounded by a random alloy has been reported recently by Stringfellow (Jen, Cherng, and Stringfellow, 1986).

A number of nonequilibrium growth processes are proving to be valuable additions to our materials preparation methods. Included in this category are all growth methods in which the substrate is held at a temperature well below the melting point of the growing material, e.g. molecular beam epitaxy (MBE), metal/organic-chemical-vapor deposition (MOCVD), and various energy-assisted epitaxies (EAE) (Green, 1983; Bicknell, Giles, and Schetzina, 1986). The EAE methods are those in which some form of energy, e.g. laser light or ion bombardment, is supplied to the growing surface. Even without energy assistance, local bonding arrangements in the layers just beneath the growth surface can reorder to attain local-minimum-free-energy

configurations driven by the energy released when the new atoms arrive and bond, typically a few eV per atom. If one thinks in terms of an effective growth surface temperature that determines the nature of the order/disorder phase state of the material, then in normal MBE and MOCVD T_{eff} probably lies below the melting temperature T_m. For liquid-phase epitaxy, one has $T_{eff} \approx T_m$, while for EAE, one has $T_{eff} > T_m$. This single T_{eff} parameter model is undoubtably an oversimplification, but it serves to establish an order among the trends of a wide range of experimental recently reported results. When T_{eff} is small (MBE and OMCVD), then correlations are high, ordered crystals and crystals with ordered arrays of domains can occur. When $T_{eff} \approx T_m$, then correlations are smaller, and depending on the alloy and composition, more nearly random arrangements or normal spinodal decomposition are more likely. When $T_{eff} \gg T_m$, then it is possible to grow materials in the form of random alloys that do not exist in equilibrium. While these materials are metastable, they may still be useful and open a whole new treasure trove to device science.

III COULOMB INTERACTIONS

This section presents a new mechanism for the alloy mixing enthalpy: the configuration-dependence of the Coulomb electron/electron interaction. Although we have formulated the problem in tight-binding theory, it can (at least in principle) be formulated in other ways. In the tight-binding theory, the driving force for the interactions are the bond polarity mismatch, in contradistinction to the customary bond length mismatch, which the Keating model characterizes. This interaction can be significant in lattice-matched materials, and, indeed, our numerical estimates (which are quite difficult to obtain reliably) are approximately the correct size to explain the now-famous experimental work of Kuan et al. (1985) on AlGaAs. The essential feature of Coulomb interactions is the configuration-dependence of charge fluctuations. Because the Coulomb energy is nonlinear in the charge density, fluctuations always increase the energy. This can be partially compensated by the long-range Madelung energy originating in a coherent sum of alternating charges. Configurations that minimize the combined effect are of lowest energy. The random configuration is always of higher energy, mainly because of the weakening of the Madelung energy. Appendix A, a reprint of van Schilfgaarde, Chen, and Sher (1986), published in *Physical Review Letters*, provides more details.

IV STRUCTURAL PROPERTIES OF COMPOUNDS AND ALLOYS

A. *Introduction*

Harrison (1980) has devised in an elegant way to obtain the total energy for tetrahedral semiconductors in tight-binding theory without recourse to integrations over the Brillouin zone. His approach starts with the bond orbital approximation, which treats the electronic structure of the solid in terms of two-center bonds, neglecting coupling between bonds and neighboring antibonds. These corrections can be restored in a systematic way in perturbation theory; Harrison terms these corrections *metallization*, because they are responsible for the delocalization of the electrons and are proportionally larger for heavier elements. The bond orbital approximation is especially attractive in the study of alloys because there is, strictly speaking, no Brillouin zone. In particular, we are interested in the elastic constants of the alloy.

In addition to the bond orbital approximation—a shortcut to the more intricate (and necessarily numerical) integration over the Brillouin Zone—Harrison has developed a theory of tight-binding matrix elements, arguing that they scale universally with free-electron bands and vary as $1/d^2$. These are purely attractive, and he adds an empirical two-body repulsive term to stabilize the crystal at its equilibrium spacing. This is postulated to vary as $1/d^4$. With these matrix elements and the repulsive term, he can calculate a wide range of structural properties in the bond orbital approximation.

Harrison's analysis, while remarkable in its simplicity, yields semiquantitative predictions of the elastic constants. This study summarizes a detailed analysis of the elastic constants in the bond orbital approximation, showing the apparent origin of the principal errors of the theory, and distinguishing the errors inherent in the bond orbital approximation and the physical approximations of the tight-binding theory.

The bond orbital approximation is found to be a reasonably accurate mathematical device; however, it does lead to inaccuracies of order 20 percent in the most polar materials. The most severe error lies in the assumed form of the two-body repulsion; this is not surprising, because it is the least well established aspect of the theory. The probable origin of the error in the two-body repulsion is the neglect of orthogonalization of the valence s and p orbitals to neighboring core wave functions. In the few cases where we have calculated the s-p orbital core interaction, the bulk modulus has agreed with experiment to within 10 percent The analysis is now being finished, and this work will be published in *Physical Review*.

B. *Analysis*

It is always possible to construct a tight-binding theory that agrees well with experiments (although quite probably one without physical foundation), by adjusting a sufficient number of parameters. One of the most elegant aspects of Harrison's analysis is its lack of adjustable parameters, in spite of its extreme simplicity. The only empirical aspect of the theory is the

assumed form of the two-body repulsion V_0, which is presumed to vary as $1/d^4$. This analysis retains all of the matrix elements of Harrison's analysis (free-electron term values for the diagonal and universal nearest-neighbor for the off-diagonal), discarding only the assumed form of the two-body repulsion. For the analysis of the elastic constants, we specify V_0 only by coefficients of a Taylor series,

$$V_0(d) = V_0(d_0) + V_0'(d_0)(d - d_0) + \tfrac{1}{2} V_0''(d_0)(d - d_0)^2 \quad , \tag{1}$$

where the linear term is fit to the equilibrium spacing and the quadratic term to the bulk modulus. As mentioned earlier, the principal contribution to the bulk modulus originates in the orthogonalization of the valence wave function to cores on neighboring sites.

Harrison (1983) discusses the analysis of the bond orbital approximation in detail. We use that analysis here with the above extension to the repulsive two-body interaction V_0.

Of the three elastic constants, the simplest to analyze is the bulk modulus, as it entails only purely radial forces (a simple compression of each bond). In the bond orbital approximation, the energy of a bond is

$$E_b = \varepsilon_c + \varepsilon_a + 2\sqrt{V_2^2 + V_3^2} + V_0 \quad , \tag{2}$$

where ε_a and ε_c are the atomic terms values of sp^3 hybrids on the anion and cation, respectively, and $V_3 = (\varepsilon_c - \varepsilon_a)/2$. It is sometimes convenient to define the quantities, following Harrison,

$$\alpha_p = \sqrt{1 - \alpha_c^2} = \frac{V_3}{\sqrt{V_2^2 + V_3^2}} \quad . \tag{3}$$

The "bond force constant," k, is related to the bulk modulus B by

$$k = \frac{\partial^2 E_b}{\partial d^2}\Big|_{d_0} = 4\sqrt{3} d_0 B \quad . \tag{4}$$

Evaluated from Eq. (2), k is

$$k = \frac{-4V_2^2(5V_3^2 + 3V_2^2)}{d_0^2(V_2^2 + V_3^2)^{3/2}} + V_0'' \quad . \tag{5}$$

There are additionally metallization corrections, but these can always be implicitly included in the two-body repulsive term. For the present analysis, V_0'' is fit to the measured bulk modulus.

Next, we examine the elastic constant $c_{11}-c_{12}$. This distortion entails only a bond-angle mismatch of Figure 4; it involves no changes in bond length. Because none of the volume-dependent quantities enter, our analysis follows exactly that of Harrison (1983). The result is, in the bond orbital approximation,

$$c_{11}-c_{12} = \sqrt{3}\alpha_c(\sqrt{3}V_{sp\sigma} + 3V_{pp\sigma} - 3V_{pp\pi})/4d_0^3 \quad . \tag{6}$$

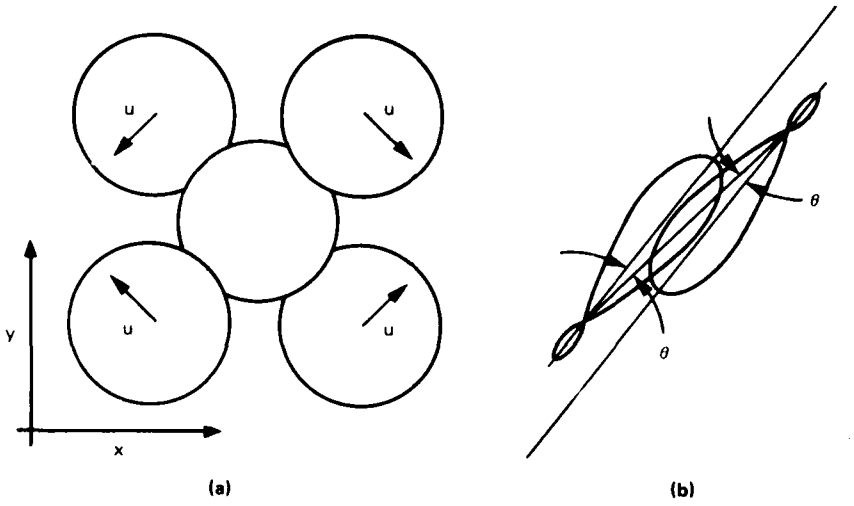

FIGURE 4 TOTAL ENERGY AS A FUNCTION OF d
(a) A single tetrahedron under a twist distortion. The neighbors at upper left and lower right are below the plane of the figure, the others above. The displacements are in the plane of the figure. (b) The misalignment of the two hybrids forming a bond, with $\theta \approx \tan\theta = u/d$.

Metallization corrections are important in the heteropolar compounds; Harrison (1983) showed that there is an important interbond metallization correction, whose effect is to alter the above result by a multiplicative factor α_c^3.

Finally we turn to the last independent elastic constant, c_{44}. It is the most difficult to handle properly because the total energy must be minimized with respect to two variational parameters, the Kleinman internal displacement parameter and (because the hybrid orbitals are no longer all equivalent) the rehybridization of the orbitals. We choose the geometry shown in Figure 5. The elastic energy takes the form

$$E = (A_{11}u'^2 + A_{12}\gamma u' + A_{13}u' + A_{22}\gamma^2 + A_{23}\gamma + A_{33})u^2 \quad , \tag{7}$$

where the variational parameters U' and γ are specified in Figure 5, and the A_{ij}s are coefficients that involve the tight-binding matrix elements. They are:

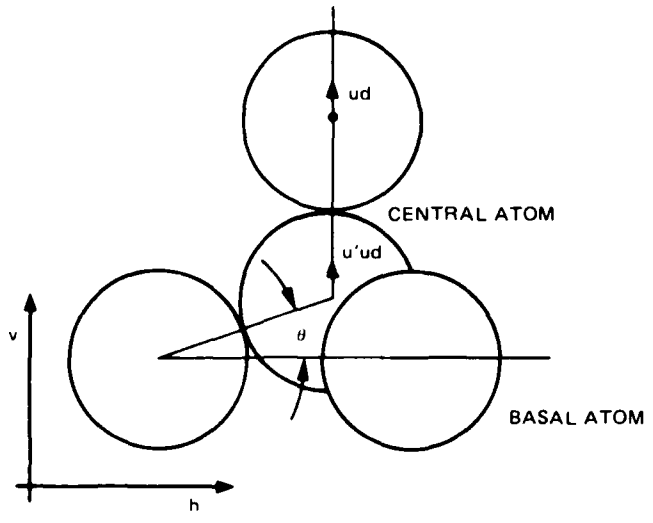

(a)

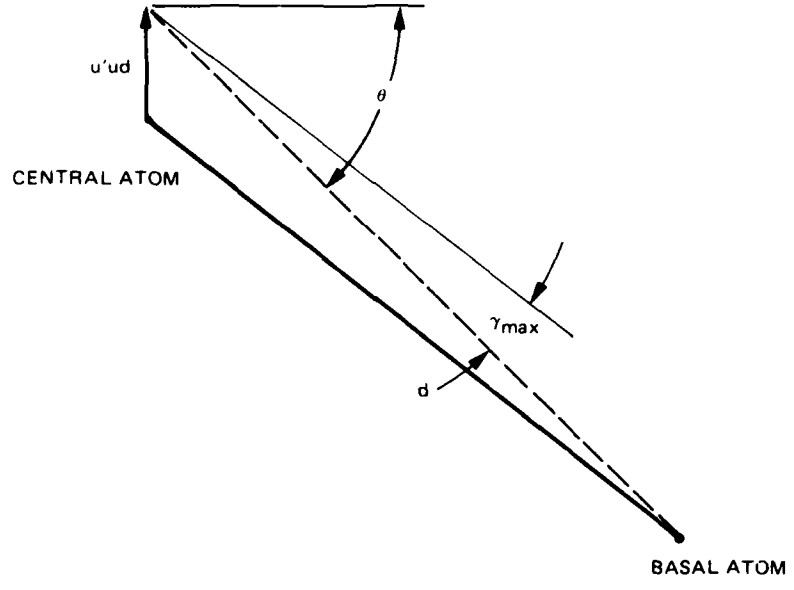

(b)

FIGURE 5 GEOMETRY WITH WHICH TO ANALYZE THE c_{44} DISTORTION

The atoms in the basal plane are frozen; the top atom is pulled vertically by u in the figure. The displacement u'ud of the central atom is not determined by symmetry, but must be minimized with respect to the total energy; the Kleinman internal displacement parameter is linearly related to u'ud. Also, the hybrid pointing to the top atom is no longer equivalent with hybirds pointing down to the basal atoms. Because of this, the basal hybrids can exchange some of their sp character with the vertical hybrid; this too is determined variationally. In one limit, the rehybridized orbital continues to point directly along the bond. That rehybridization angle is illustrated in Figure 5(b) as γ_{max}. The rigid hybrid approximation sets γ to zero; the variationally determined gamma is typically 1/3 γ_{max} in covalent materials.

$$A_{11} = \frac{[(16\sqrt{3}V_{sp\sigma} + 48V_{pp\sigma} - 48V_{pp\pi})\ \alpha_c^3 + 12d_0^2k]}{9} \tag{8}$$

$$A_{22} = 2(7\sqrt{3}V_{sp\sigma} + 3V_{pp\sigma} - 3V_{pp\pi}) \tag{9}$$

$$A_{33} = d_0^2k \tag{10}$$

$$A_{12} = -4\sqrt{2}\alpha_c(-4\sqrt{3}V_{sp\sigma} - 12V_{pp\sigma} - 6V_{pp\pi} - 18V_2)/3 \tag{11}$$

$$A_{13} = -2d^2k \tag{12}$$

$$A_{23} = -6\sqrt{2}\alpha_c[\sqrt{3}(1 + \alpha_p^2)(V_{sp\sigma} + V_{pp\sigma} + V_2) - 3\alpha_c\alpha_p\ \Delta V_1] \quad . \tag{13}$$

The coefficients A_{12} and A_{22} are too complicated to display compactly in the heteropolar compounds and are only shown here in the covalent case. As in the elastic constant c_{11}–c_{12}, the portion of A_{11} proportional to α_c^3 should be proportional only to α_c in the bond orbital approximation; the same interbond metallization corrections in c_{11}–c_{12} apply here. The remaining important metallization corrections are included implicitly as modifications to the two-body repulsive term.

Table 1 shows the calculated elastic constants for the elemental semiconductors. It is seen that both c_{11}–c_{12} and c_{44} are well predicted, and that the Kleinman internal displacement parameter agrees considerably better with experiment than does Harrison's analysis. This shows that the principal error in Harrison's formulation of c_{44} is due to his form of V_0. The remaining errors can be taken as a measure the uncertainty of the universal matrix elements. The matrix elements, for example, were obtained with a peripheral s state (which, however, was not included in the calculation of the elastic constants; its effect is to weaken V_{sp}). The elastic constants c_{11}–c_{12} and c_{44} increase by about 5 percent if V_{sp} is fit instead without a peripheral state.

Alternatively, this good agreement with experiment shows that matrix elements do scale nearly as free electron matrix elements from one material to another. However, this analysis tells very little about the variation of the matrix element with bond length for a given material (also assumed by Harrison to vary as $1/d^2$). We have also formulated the theory using the form of the universal matrix elements, but allowing for an arbitrary variation with bond length (specifying it by a Taylor series, as in the V_0). c_{44} exhibits an extremely weak dependence on the first derivative of the matrix elements, $\partial V_2/\partial d$ and is completely independent of the second derivative.

Table 1

CALCULATED ELASTIC CONSTANTS

Numbers in parentheses are corresponding experimental values

Material	D	B	c_{11-12}	c_{44}	Kleinman
C	1.54 (1.54)	44.20 (44.20)	67.10 (95.10)	47.37 (57.70)	
Si	2.35 (2.35)	9.78 (9.78)	8.11 (10.20)	6.95 (7.96)	0.58* (0.63, 0.73)
Ge	2.44 (2.44)	7.52 (7.52)	6.72 (8.06)	5.65 (6.71)	

*Harrison is 0.43

For the ionic semiconductors, the analysis of c_{44} becomes strongly dependent on several rather uncertain quantities, such as the difference in V_1 between the cation and anion. This quantity is quite sensitive to the atomic term values used, a quantity that is not known well in any case.

To avoid this difficulty, we simplify the above analysis to the "rigid hybrid" approximation: we set γ in Eq. (7) to zero, and thus require that the four hybrids be rigid. This overestimates the force constants in all cases, but eliminates the troublesome coefficients A_{12} and A_{22}, and the strong dependence on V_1. The errors introduced in the covalent case are not severe, as Table 2 shows. It is also seen that $c_{11}-c_{12}$ and c_{44} exhibits reasonably good agreement with experiment, but overestimate somewhat the dependence on polarity. This is directly attributable to the bond orbital approximation itself, as the bond orbital approximation tends to overestimate the polarity in ionic materials [Berding, unpublished work]. We obtained the polarities by numerical integration over the Brillouin zone, and re-evaluated the elastic constants substituting these polarities instead of those calculated by the bond orbital approximation. The resulting elastic constants, shown in Table 3, exhibit small and consistent departures from experiment.

The agreement overall is excellent and establishes strong experimental support for both the bond orbital approximation and the universal tight-binding theory.

The extension of this theory to alloys involves appreciation of the fact that there are distortions of each cluster in the alloy because their volume does not match the average volume per cluster of the alloy medium. As a consequence, the local bonds in the cluster are strained. Thus, the elastic moduli correspond to responses to stresses about the prestrained positions. Moreover, there is a long-range strain field in the medium caused by each cluster. It is well known that if a segment of an elastic medium is removed and replaced by one of a different size, then the net volume change of the sample is greater than the difference in volume between the removed and replaced segments. Therefore, there is both a core and a long-range contribution to the modification of average elastic constants in a medium. The long-range contribution is complicated by interactions among the strain fields produced by different clusters. We are attempting to sort through the problem at present.

Table 2

ELASTIC CONSTANTS: RIGID HYBRID APPROXIMATION

Material	d (Å)	α_p	B (10^{11} erg/cm^3)	c_{11-12} (10^{11} erg/cm^3)	c_{44} (10^{11} erg/cm^3)
C	1.54	0.00	44.20	67.10	57.12
	(1.54)	(--)	(44.20)	(95.10)	(57.70)
Si	2.35	0.00	9.78	8.11	9.34
	(2.35)	(--)	(9.78)	(10.20)	(7.96)
AlP	2.36	0.52	8.60	4.91	6.52
	(2.36)	(--)	(8.60)	(5.90)	(6.15)
AlAs	2.43	0.52	7.73	4.25	5.71
	(2.43)	(--)	(7.73)	(6.16)	(5.42)
AlSb	2.66	0.48	5.93	2.94	4.08
	(2.66)	(--)	(5.93)	(4.50)	(4.16)
GaP	2.36	0.50	8.87	5.17	6.81
	(2.36)	(--)	(8.87)	(7.88)	(7.05)
ZnS	2.34	0.65	7.80	3.66	5.16
	(2.34)	(--)	(7.80)	(3.90)	(4.62)
GeGe	2.44	0.00	7.52	6.72	7.49
	(2.44)	(--)	(7.52)	(8.06)	(6.71)
GaAs	2.45	0.50	7.48	4.25	5.65
	(2.45)	(--)	(7.48)	(6.48)	(5.92)
ZnSe	2.45	0.67	5.95	2.68	3.83
	(2.45)	(--)	(5.95)	(3.22)	(4.41)
GaSb	2.65	0.44	5.63	3.20	4.25
	(2.65)	(--)	(5.63)	(4.82)	(4.32)
ZnTe	2.64	0.68	5.09	1.79	2.73
	(2.64)	(--)	(5.09)	(3.06)	(3.12)
InP	2.54	0.59	7.25	2.88	4.26
	(2.54)	(--)	(7.25)	(4.46)	(4.60)
InAs	2.61	0.59	5.80	2.52	3.64
	(2.61)	(--)	(5.80)	(3.80)	(3.96)
InSb	2.81	0.54	4.66	1.98	2.88
	(2.81)	(--)	(4.66)	(3.02)	(3.02)
CdTe	2.81	0.73	4.24	1.08	1.76
	(2.81)	(--)	(4.24)	(1.68)	(1.99)

Table 3

ELASTIC CONSTANTS: RIGID HYBRID APPROXIMATION
WITH CORRECTED POLARITIES

Material	d (Å)	α_p	B (10^{11} erg/cm^3)	c_{11-12} (10^{11} erg/cm^3)	c_{44} (10^{11} erg/cm^3)
C	1.54	0.00	44.20	67.10	57.12
	(1.54)	(--)	(44.20)	(95.10)	(57.70)
Si	2.35	0.00	9.78	8.11	9.34
	(2.35)	(--)	(9.78)	(10.20)	(7.96)
AlP	2.36	0.43	8.60	5.84	7.29
	(2.36)	(--)	(8.60)	(5.90)	(6.15)
AlAs	2.43	0.40	7.73	5.32	6.60
	(2.43)	(--)	(7.73)	(6.16)	(5.42)
AlSb	2.66	0.	5.93	3.70	4.76
	(2.66)	(--)	(5.93)	(4 50)	(4.16)
GaP	2.36	0.39	8.87	6.22	7.66
	(2.36)	(--)	(8.87)	(7.88)	(7.05)
ZnS	2.34	0.57	7.80	4.62	6.06
	(2.34)	(--)	(7.80)	(3.90)	(4.62)
GeGe	2.44	0.00	7.52	6.72	7.49
	(2.44)	(--)	(7.52)	(8.06)	(6.71)
GaAs	2.45	0.35	7.48	5.40	6.58
	(2.45)	(--)	(7.48)	(6.48)	(5.92)
ZnSe	2.45	0.56	5.95	3.77	4.82
	(2.45)	(--)	(5.95)	(3.22)	(4.41)
GaSb	2.65	0.29	5.63	3.92	4.84
	(2.65)	(--)	(5.63)	(4.82)	(4.32)
ZnTe	2.64	0.55	5.09	2.66	3.63
	(2.64)	(--)	(5.09)	(3.06)	(3.12)
InP	2.54	0.47	7.25	3.81	5.20
	(2.54)	(--)	(7.25)	(4.46)	(4.60)
InAs	2.61	0.43	5.80	3.56	4.61
	(2.61)	(--)	(5.80)	(3.80)	(3.96)
InSb	2.81	0.35	4.66	2.73	3.59
	(2.81)	(--)	(4.66)	(3.02)	(3.02)
CdTe	2.81	0.59	4.24	1.76	2.57
	(2.81)	(--)	(4.24)	(1.68)	(1.99)

V ANGULAR DEPENDENCE OF THE HARDNESS

We have begun to incorporate anisotropicity into a theory of hardness in which the hardness is determined by the interaction energy among dislocations generated by an indentation (Sher, Chen, and Spicer, 1985). Several aspects of anisotropicity have been observed experimentally and are being addressed in our study:

(1) In fcc, diamond, and zincblende structures slip is observed to occur most often on {111} planes in the $<\bar{1}10>$ directions. The effective shear coefficient, G, which enters into our theory of hardness should correspond to this slip system. Duncan and Kuhlmann-Wilsdorf (1967) have derived an analytic solution for the effective strain coefficient for the $\{111\}$ $<\bar{1}10>$ slip system. Based on this slip system, the picture of the dislocation configuration in our theory of hardness needs to be modified, so for a given orientation of the indentor slip is permitted only in the preferred directions. Then, the lowest-energy-dislocation configuration needs to be found with this extra constraint to find the lower bound on the hardness.

(2) In germanium and InSb, the microhardness has been observed to vary from one crystalographic plane to another, with (111) surface the hardest, (110) the softest. The observe increase in hardness from the (110) to the (111) plane is 15 percent in germanium, but only 5 percent in InSb (Ablova, 1961; Ablova and Feostiskova, 1963). As discussed above, the picture of the dislocation configuration generated by the indenter needs to be modified; the minimum energy dislocation pattern will differ from the (111) to the (110) face. For example, the (110) face has two slip planes which are perpendicular to the surface and two slip planes at 35° angles to the surface. The (111) surface, in comparison, has three equivalent slip planes at 70.5° angles to the surface. In addition, the (111) surface is itself a slip plane.

(3) The scratch hardness on the (111) surface of InSb shows a three-fold symmetry. The maximum and minimum occur in $<11\bar{2}>$ directions. The implication of the three-fold symmetry is that in the $<11\bar{2}>$ directions, a scratch in one direction will result in a different hardness than scratching in the opposite direction. Scratch hardness, therefore, necessarily involves a component of force in the plane of the surface, along the scratching direction. We are not currently addressing scratch hardness.

VI VACANCY-FORMATION ENERGY

The present status of our efforts to understand vacancy-formation energies is contained in the preprint of a paper attached as Appendix A. We are currently generalizing the results to all semiconductor alloys and considering a number of final states for the removed atoms.

REFERENCES

Ablova, M.S., 1961: *Soviet Phys. Solid State*, Vo. 3, No. 6, p. 1320.

Ablova, M.S., and N.N. Feoktistova, 1963: *Soviet Phys. Solid State*, Vol. 5, No. 1, p. 265.

Bevk, J., J.P. Mannaerts, L.C. Feldman, and B.A. Davidson, 1986: *Appl. Phys. Lett.*, Vol. 49, p. 286.

Bicknell, R.N., N.C. Giles, and J.F. Schetzina, 1986: *Appl. Phys. Lett.*, Vol. 49, p. 1095.

Chen, A.-B., and A. Sher, 1985a: *Mat. Res. Symp. Proc.*, Vol. 46, p. 137.

Chen, A.-B., and A. Sher, 1985b: *Phys. Rev.*, Vol. B32, p. 3695.

Czyzyk, M.T., M. Podgorny, A. Balzarotti, P. Lelardi, N. Motta, A. Kisiel, and M. Zemnal-Slarnawska, 1986: *Z. Phys. B—Cond. Matter*, Vol. 62, p. 153.

Duncan, T., and D. Kuhlmann-Wilsdorf, 1967: *J. Appl. Phys.*, Vol. 38, No. 1, p. 313.

Green, J.E., 1983: *J. Vac. Sci. Technol. B*, Vol. 1, p. 229.

Guggenheim, E.A., 1952: *Mixtures* (Oxford at the Clarendon Press).

Harrison, W.A., 1980: *Electronic Structure and Properties of Solids* (Freeman, San Francisco).

Harrison, W.A., 1983: *Microscience* (SRI International publication), Vol. 3, p. 35.

Jen, H.R., M.J. Cherng, and G.B. Stringfellow, 1986: 7th International Conference on Ternary and Multinary Compounds, Snowmass, Colorado, 10-12 September 1986.

Kuan, T.S., T.F. Kuech, W.I. Wang, and E.L. Wilkie, 1985: *Phys. Rev. Lett.*, Vol. 54, p. 201.

Muller, M.W., 1984: *Phys. Rev. B*, Vol. 30, p. 6196.

Sher, A., A.-B. Chen, and M. van Schilfgaarde, 1986: *J. Vac. Sci. Technol.*, Vol. A4, p. 1965.

Sher, A., A.-B. Chen, and W.E. Spicer, 1985: *Appl. Phys. Lett.*, Vol. 46, p. 54.

Srivastava, G.P., J.L. Martins, and A. Zunger, 1985: *Phys. Rev. B*, Vol. 31, p. 2561.

van Schilfgaarde, M., A.-B. Chen, and A. Sher, 1986: *Phys. Rev. Lett.*, Vol. 57, p. 1149.

Appendix A

REPRINT OF "COULOMB ENERGY IN PSEUDOBINARY ALLOYS"

Coulomb Energy in Pseudobinary Alloys

Mark van Schilfgaarde
SRI International, Menlo Park, California 94025

An-Ban Chen
Department of Physics, Auburn University, Auburn, Alabama 36849

and

A. Sher
SRI International, Menlo Park, California 94025

(Received 6 May 1986)

A tight-binding theory is derived for Coulomb electron-electron interactions in tetrahedrally coordinated pseudobinary alloys of the form $A_{0.5}B_{0.5}C$. Coulomb contributions to the mixing enthalpy are driven by the *bond polarity* mismatch, as distinct from the *bond length* mismatch customarily considered. The Coulomb energy shows a strong dependence on the alloy configuration, which arises from the configuration dependence of charge fluctuations. The mixing enthalpy is of order 0.10 eV, commensurate with that of the strain contribution customarily considered.

PACS numbers: 64.80.−v, 64.75.+g, 81.30.Hd

On a zinc-blende lattice, the energetics that give rise to nonrandom distributions of alloy constituents have long been associated with incoherent strain fields due to the lattice mismatch of the constituents. However, there is recent experimental evidence[1] that the cations in AlGaAs exhibit long-range order. Also, a 7-meV mixing enthalpy has been measured in HgCdTe. Both materials are lattice matched, and this indicates that at least one alternative mechanism plays an important role in the alloy mixing enthalpy. Presented here is the first explicit calculation of the electron-electron Coulomb contribution to the mixing enthalpy in tetrahedrally coordinated pseudobinary alloys of the form $A_{0.5}B_{0.5}C$. It is found to be large and quite comparable to the energies associated with lattice mismatch. We consider here the configuration dependence of the direct (Hartree) term in the electron-electron Coulomb interaction, which can be understood in terms of charge fluctuations driven by the differing potentials of the A and B atoms.

Coulomb interactions[2] are formulated in the tight-binding bond orbital approximation,[3,4] in terms of an effective intra-atomic contribution $U_{\rm eff}$ and an interatomic "Madelung" contribution $K_{\rm eff}$. Both $U_{\rm eff}$ and $K_{\rm eff}$ depend on the particular configuration of the alloy, and the net interaction takes the form

$$(U_{\rm eff}-K_{\rm eff})(\Delta Z)^2, \tag{1}$$

where ΔZ is half the difference in charge transfer in the two alloy bonds, determined by the bond polarity difference. Equation (1) makes a contribution to the mixing enthalpy in proportion to $(\Delta Z)^2$ in contradistinction to the customary treatment which focuses on the strain contribution and varies in proportion to the square of the bond length mismatch, $(\Delta d)^2$. [There are also contributions in proportion to $(\Delta Z)(\Delta d)$. They are not considered here.] $U_{\rm eff}-K_{\rm eff}$ is calculated for the $A_{0.5}B_{0.5}C$ in three configurations: (a) a random alloy, (b) the pure AC and BC materials, and (c) an ordered phase in which the two alloy constituents A and B lie in alternating [100] planes. In the cation-substituted alloys, $U_{\rm eff}-K_{\rm eff}$ is near zero for both of the ordered configurations considered, but ~ 1.5 eV for a random configuration, leading to a positive contribution to the mixing enthalpy. Since ΔZ can be of order 0.2, the Coulomb contribution to the mixing enthalpy can be of order 50 meV, quite commensurate with the strain contribution.

We calculate the Coulomb contributions in the bond orbital approximation, which neglects coupling between bonds and neighboring antibonds,[3] and allows us to treat the charge transfer of each bond independently. This approximation is not essential but simplifies the analysis, as it allows us to calculate the net charge transfer at a particular site as a sum of charge transfers from each bond. We include only the direct terms in the Coulomb interactions.[5] Harrison[2] has studied Coulomb interactions in the pure crystal, and has argued that their principal correction to the classical tight-binding Hamiltonian is to add a correction proportional to U to the site energy, compensated by an interatomic "Madelung" energy K.

To treat the intra-atomic U, consider an isolated atom. Because of the electron-electron interaction the potential varies with the charge Z, and the energy E is nonlinear in Z. The coefficient to the linear term of an expansion of $E(Z)$ about $Z=0$ (corresponding to

the neutral atom), $-\epsilon \equiv (\partial E/\partial Z)_0$, is in Hartree-Fock theory the term value, since it is the change in energy with respect to occupation. We account for the Coulomb interaction with an energy dependence

$$E(Z) \approx -\epsilon Z + \tfrac{1}{2} UZ^2 + \text{const}, \tag{2}$$

where

$$U = e^2 \int d^3r_1\, d^3r_2 \psi^2(r_1)(1/r_{12})\psi^2(r_2).$$

(See the Appendix for further discussion and numerical evaluation of U and K.) Substituting Eq. (2) for the usual Hartree-Fock term values into the bond orbital approximation leads to Coulomb corrections of the form

$$[\tfrac{1}{2}(U_a + U_c) - K]Z^2 \equiv U^* Z^2 \tag{3}$$

per atom pair. Here Z is the cation-anion charge transfer, and U_a and U_c are the intra-atomic electron-electron Coulomb repulsion on the anion and cation sites, respectively. K is the interatomic direct term, the "Madelung" energy $-1.64e^2/d$ for bond length d, if the atomic charge distributions do not overlap (see Appendix).

If the solution is not carried out self-consistently, Eq. (3) adds directly to the total energy. Solved self-consistently, the Coulomb correction is, to second order in U^*, $U^*Z^2(1+4\alpha_c^3 U^*/|V_2|)$, where the covalency α_c and the hybrid matrix element V_2 are defined as in Refs. 3 and 4. Because U^*/V_2 is small, we drop self-consistency corrections and carry out the analysis to first order only. In practice, Z for each bond is calculated from Harrison's bond orbital approximation with a correction for metallization,[3,4] the second-order coupling between bonds and antibonds.

We consider an $A_{0.5}B_{0.5}C$ alloy and define the charge transfer in the AC and BC bonds as Z_A and Z_B, respectively, and define the virtual-crystal average $\bar{Z} \equiv (Z_A + Z_B)/2$ and *fluctuation* $\Delta Z \equiv (Z_A - Z_B)/2$. All configuration dependence is most easily interpreted in terms of charge fluctuations; it is for this reason that the configuration dependence takes the form Eq. (1). In the virtual crystal, each site has an average charge $\pm\bar{Z}$. There are no charge fluctuations, and the Coulomb energy is that of the average material, $U^*\bar{Z}^2$.

In the bond orbital approximation, every A atom has the same charge, as does every B atom. The C atom has one of five charge states, depending on the number of A and B atoms surrounding it. Because there are only a finite number of charge states, both the intra-atomic and interatomic "Madelung" energy of the entire lattice can be obtained for any configuration of alloy atoms. The Coulomb energy per atom pair of the separate compounds AB and BC can be written out of hand,

$$\begin{aligned} E_{\text{separate phases}} &= U^* \tfrac{1}{2}(Z_A^2 + Z_B^2) \\ &= U^*[\bar{Z}^2 + (\Delta Z)^2], \end{aligned} \tag{4}$$

and differs from that of the virtual crystal because each charge fluctuates by $\pm\Delta Z$ relative to that of the virtual crystal.

We next consider a random alloy, choosing a cation-substituted alloy to facilitate discussion. The Madelung energy is obtained by summing of the Coulomb pair potentials over all sites μ and ν. It differs from that of the virtual crystal by

$$\frac{e^2}{2}\sum_{\mu\nu}\frac{1}{d_{\mu\nu}}\left[\sum_{ij} P_i(\mu) Z_i(\mu) P'_{j|i}(\nu) Z_j(\nu) - \bar{Z}(\mu)\bar{Z}(\nu)\right], \tag{5}$$

where $P_i(\mu)$ is the probability of site μ having charge $Z_i(\mu)$ and $P'_{j|i}(\nu)$ is the conditional probability of site ν having charge Z_j when $Z_i(\mu)$ is specified. When $P'_{j|i}(\nu)$ is independent of i, the sums over i and j factor and the quantity in brackets vanishes identically. Since in the bond orbital approximation the charges on the alloy sublattice are statistically independent, the only correlated pairs are nearest-neighbor pairs and second-neighbor anion-anion pairs (correlated through their common cation).

Considering first the nearest-neighbor pair (using a cation-substituted alloy for notational convenience), there are five possible anion charge states, which we label $i = 0$–4, signifying the number of cation neighbors of type A. The anion charge differs from the virtual crystal by ΔZ, $\Delta Z/2$, 0, $-\Delta Z/2$, and $-\Delta Z$ for these five states. In a random alloy, the probabilities P_i of finding these states are $\frac{1}{16}$, $\frac{4}{16}$, $\frac{6}{16}$, $\frac{4}{16}$, and $\frac{1}{16}$, respectively. The conditional probabilities $P'_{A|i}$ and $P'_{B|i}$ of finding cation neighbors of type A and B are $i/4$ and $(4-i)/4$.

Consider next the nearest anion-anion neighbors. The separate probabilities of each anion possessing a given charge state are statistically dependent for nearest anion-anion neighbors through the cation neighbor that they share in common. Given the charge Z_i on one site, the conditional probability of finding a charge Z_j on the neighboring anion site is mediated through the conditional probability of the common cation by $P'_{j|i} = P'_{A|i}P'_{j|A} + P'_{B|i}P'_{j|B}$. The intra-atomic contributions can be similarly summed relative to the virtual crystal as $\sum_i P_i[E(Z_i) - E(\bar{Z})]$

and the net Coulomb energy is

$$U^*\bar{Z}^2+\left(\frac{1}{8}U_a+\frac{1}{2}U_c-\frac{4}{4}\frac{e^2}{d}+\frac{12}{16}\frac{e^2}{(8/3)^{1/2}d}\right)(\Delta Z)^2\equiv U^*\bar{Z}^2+U_{\rm ran}(\Delta Z)^2. \quad (6)$$

Again, each term has a simple interpretation in terms of charge fluctuations. Fluctuations on the anion sites are $\frac{1}{4}$ as large as in Eq. (4); this reduces the intra-atomic anion and the nearest-neighbor interatomic contributions to $\frac{1}{4}$, and each of the twelve nearest-neighbor anion-anion fluctuations to $\frac{1}{16}$ of Eq. (4).

We finally consider a sublattice of cations which are ordered by arrangement of the A and the B atoms in alternating layers in the [100] planes.[1] There is an additional Madelung energy in the A-B sites (which we calculate by an Ewald sum), but no charge fluctuation on the C site since every C site is in the same environment. The Coulomb energy is then

$$U^*\bar{Z}^2+\frac{1}{2}\left(U_c-\frac{1.59e^2}{(8/3)^{1/2}d}\right)(\Delta Z)^2\equiv U^*\bar{Z}^2+U_{100}(\Delta Z)^2. \quad (7)$$

The difference in Coulomb energies of the three configurations considered, Eqs. (4), (6), and (7), differ only in terms due to charge fluctuations, their difference taking the form Eq. (1). Numerical estimates (see Appendix) of the effective U's and ΔZ are shown in Table I. In the cation-substituted alloy, the Coulomb energy of the random alloy is approximately $1.5(\Delta Z)^2$ eV larger than that of the separated materials. When ΔZ is 0.2, the mixing energy is 0.06 eV—a large mixing energy. In the anion-substituted alloys, the mixing energy is somewhat larger, $2.5(\Delta Z)^2$ eV. The generally higher energy of the random configuration can be understood as a diminution in the interatomic electrostatic energy. Without the long-range order there is no Madelung "enhancement" of the electrostatic energy gained from a coherent sum of alternating charges.

In the cation-substituted alloys, the Coulomb energies of the two ordered configurations are indistinguishable within the accuracy of the theory. There is apparently no significant penalty from the Coulomb interactions; they do not prevent the ordered sublattice from being a stable configuration. The situation changes in the anion-substituted alloys, where the ordered sublattice has higher energy than the pure materials. The asymmetry in the anion-substituted and cation-substituted alloys is due to the fact that the anion has larger intra-atomic Coulomb energy U of some 2 eV. In real cation-substituted alloys, kinetic barriers may favor the sublattice over the separate materials, especially if the energies are comparable. The path from an initial random configuration (as is roughly the situation experimentally) to the pure materials (spinodal decomposition) becomes progressively more complicated as the correlation length increases, while this is not so for the ordered sublattice. Therefore, when the energy of a random configuration is high in comparison to the ordered configurations as it is here, the ordered sublattice may be the favored configuration experimentally. This is particularly true in the present case because the interactions are long ranged. It takes a rather long correlation length for the lattice to gain a substantial portion of the Madelung "enhancement" from a coherent sum of ordered alter-

TABLE I. Numerical estimates of the Coulomb energies, in electronvolts, in three configurations of selected alloys $A_{0.5}B_{0.5}C$, as outlined in the text. U_c and U_a are the intra-atomic interactions used in the calculations, and U^* is given by Eq. (5). The charge-fluctuation dependence in the Coulomb energy for the pure materials [Eq. (4)], the random alloy [Eq. (6)], and the ordered sublattice [Eq. (7)] are given by the columns U^*, $U_{\rm ran}$, and U_{100}, each column multiplied by $(\Delta Z)^2$. The mixing energy is thus $\Delta E=(U_{\rm ran}-U^*)(\Delta Z)^2$. For the $A_{0.5}B_{0.5}C$ composition, the "mixing enthalpy parameter" Ω_p is $4\Delta E$.

	U_c	U_a	U^*	U_{100}	$U_{\rm ran}$	ΔZ
AlGaP	6.48	9.92	0.35	0.27	1.72	0.03
AlInP	6.07	9.92	0.35	0.17	1.60	-0.17
GaInP	6.26	9.92	0.36	0.27	1.67	-0.20
AlGaAs	6.48	9.49	0.33	0.37	1.74	0.02
AlInAs	6.07	9.49	0.33	0.25	1.61	-0.17
GaInAs	6.26	9.49	0.34	0.36	1.69	-0.19
AlGaSb	6.48	8.10	0.31	0.60	1.80	0.05
AlInSb	6.07	8.10	0.30	0.47	1.66	-0.16
GaInSb	6.26	8.10	0.31	0.56	1.74	-0.21
AlPAs	6.28	9.71	0.33	1.93	2.94	0.03
GaPSb	6.67	8.98	0.32	1.69	2.70	0.18
InAsSb	5.89	8.77	0.33	1.80	2.68	0.13
AlPAs	6.28	9.71	0.33	1.93	2.94	0.03
AlPSb	6.28	8.98	0.31	1.69	2.69	0.16
AlAsSb	6.28	8.77	0.30	1.63	2.63	0.13
GaPAs	6.67	9.71	0.35	1.94	2.94	0.03
GaPSb	6.67	8.98	0.32	1.69	2.70	0.18
GaAsSb	6.67	8.77	0.32	1.64	2.63	0.15
InPAs	5.89	9.71	0.37	2.13	3.00	0.03
InPSb	5.89	8.98	0.34	1.87	2.75	0.17
InAsSb	5.89	8.77	0.33	1.80	2.68	0.13
ZnCdTe	4.99	9.36	0.28	-0.08	1.25	-0.09
ZnHgTe	4.90	9.36	0.28	-0.13	1.22	-0.01
CdHgTe	4.73	9.18	0.26	-0.13	1.17	0.08

nating charges. Thus the Coulomb interactions have in principle all of the ingredients to account for the long-range ordering found experimentally in $Al_{0.5}Ga_{0.5}As$.[1] However, our calculated value of ΔZ in Table I is too small to account for the ordering; this is because the Hartree-Fock atomic term values that we use for Al and Ga are so similar that this elementary tight-binding theory cannot distinguish between Al and Ga. It is quite possible however, that a more sophisticated tight-binding theory can explain the ordering found experimentally. This has not been explored.

Finally, we remark on the role of Coulomb interactions in HgCdTe, a II-VI compound. (HgCdTe is an interesting case because it has a 7-meV mixing enthalpy but no significant lattice mismatch.) Usually a large bond polarity difference coincides with a large lattice mismatch because the atomic size and the atomic term values are closely correlated. Hg is an exception to this because its s state is deepened by relativistic effects, and HgCdTe has a significant bond polarity difference. The Coulomb mixing enthalpy as estimated from Table I is 6 meV,[6] showing that the Coulomb energies are large enough to be responsible for the observed mixing enthalpy.

Most alloy calculations are carried out in a cluster approximation, which divides the lattice into clusters and assigns an energy to each cluster that is taken to be independent of the surrounding clusters. Because the Coulomb interaction is long ranged on the scale of a bond length, small clusters may in fact depend strongly on the surroundings. Virtually all present-day calculations embed clusters in either a virtual crystal or a supercell to obtain cluster energies. This work indicates that in many cases such an approximation may be quite poor, particularly for small clusters. The smallest cluster size that is reasonably configuration independent has not yet been determined.

In conclusion, we have developed an elementary theory for the configuration dependence of Coulomb interactions in semiconductor alloys. Numerical calculations show that they make an important contribution to the mixing energy. They arise from the configuration dependence of charge fluctuations, and depend on bond polarity mismatch, and must be added to the lattice-mismatch energies customarily believed to be responsible for ordering the alloy sublattice.

We wish to thank W. A. Harrison for helpful suggestions and for reading the manuscript. This work was supported in part by U.S. Air Force Office of Scientific Research Contract No. F49620-85-C-0023 and U.S. Office of Naval Research Contract No. N00014-85-K-0448.

Note added.—An *ab-initio* linear-muffin-tin-orbital calculation was performed on AlAs and GaAs. The difference in anion-cation charge transfer was found to be approximately 0.1, leading to a significant Coulomb mixing enthalpy of 14 meV.

Appendix: numerical estimates of U and K.—The nonlinearity in $E(Z)$, Eq. (2), arises from the potential change due to the electron-electron Coulomb interaction, but the wave functions will also relax because of this change. One can estimate the importance of corrections beyond the direct Coulomb interaction U by comparing the calculated U to the difference between the experimental ionization potential and the electron affinity, i.e., $[E(1)-E(0)]-[E(0)-E(-1)]$. Harrison[2] obtained his values for U by interpolating experimental data on the first and second ionization potentials. From calculated atomic wave functions using a density-functional program,[7] we calculated U from the direct Coulomb repulsion in the valence p orbital. The resulting values of U agreed within a few percent with Harrison's tabulated values, but overestimated slightly the variation with row and column. Table I shows the values of U obtained in this way.

Harrison used the same value of U in the solid. In the calculation of the Madelung energy, he neglected the charge overlap, underestimating $U-K$ by 2–3 eV. In the present calculation it is essential that U and K be calculated on an equal footing, and we have chosen here to approximate the charge density with a superposition of free-atomic charges. In this way we retain the free-atomic U, but the charge overlap in any nearest-neighbor contribution to the interatomic interaction must be explicitly taken into account. In the present work only the valence p orbitals are used to calculate U. In a solid, unlike the atom, the occupancy of the s orbital also depends on the charge, and this would need to be considered in a more complete formulation.

[1]T. S. Kuan, T. F. Kuech, W. I. Wang, and E. L. Wilkie, Phys. Rev. Lett. **54**, 201 (1985).

[2]W. A. Harrison, Phys. Rev. B **31**, 2121 (1985).

[3]W. A. Harrison, Phys. Rev. B **27**, 3592 (1983).

[4]W. A. Harrison, Microscience **3**, 35 (1983) (published by SRI International).

[5]A more rigorous treatment of the Coulomb interactions would require evaluation of all Coulomb terms

$$U_{ijkl}=e^2\int d^3r_1\,d^3r_2\,\psi_i^*(r_1)\,\psi_j^*(r_2)(1/r_{12})\psi_k(r_1)\psi_l(r_2),$$

and would also have to treat relaxation of the wave functions as charge is added. C. Huang, J. A. Moriarty, and A. Sher [Phys. Rev. B **14**, 2539 (1976)] have shown that, at least in a two-electron bond orbital approximation, by far the dominant corrections are the direct terms, and in the present work we consider only them.

[6]The calculated value is probably fortuitously close to the experimental value, since the bond charge transfer apparently depends on the bond environment (K. Haas, private communication) reflecting a significant interbond coupling that the bond orbital approximation neglects.

[7]J. P. Desclaux, Comput. Phys. Commun. **1**, 216 (1970).

Appendix B

REPRINT OF "VACANCY FORMATION ENERGIES IN II-VI SEMICONDUCTORS"

VACANCY FORMATION ENERGIES IN II-VI SEMICONDUCTORS

M.A. Berding and A. Sher

SRI International, Menlo Park, California 94025

A.-B. Chen, Auburn University, Auburn, Alabama 36801

ABSTRACT

The cation and anion vacancy formation energies are calculated for HgTe, ZnTe and CdTe and their alloys using a tight-binding cluster Hamiltonian. Neutral vacancies only have been assumed and two final states of the removed atom have been considered; a free atom in vacuum, and an atom on a (111) A or B surface. Corrections caused by rehybridization of the dangling bonds and Coulomb energies resulting from charge redistribution have been included.

I. INTRODUCTION

Vacancies affect many electrical properties in semiconductors; for example, they serve as largely uncontrolled dopants and impact the electron and hole mobilities. Structural properties are also sensitive to the presence of vacancies; dislocation formation and propagation, and self and impurity diffusion depend on vacancy concentrations. Experimentally, the quantity most measured is the vacancy activation energy ΔE_a, which is the sum of a vacancy formation energy ΔE_v, and a vacancy migration energy ΔE_m.

The theory of defect structures has advanced considerably in recent years, particularly with the self-consistent Green's function technique (SCGF).[1-3] While SCGF calculates the difference in total energies accurately, e.g. the migration energy, the accuracy for the absolute energy is not better than ~ 1 eV. In addition, SCGF would have difficulty dealing with semiconductor alloys because of the lack of translational symmetry in alloy systems. The simulation of defects and their environments by clusters have not been completely successful in determining the energy levels in the gap; even for localized defect potentials, the defect wave functions have not been found to be well localized within clusters of up to 71 atoms.[4] Hence, there is uncertainty in determining energy levels in the gap.

Many of the electrical and structural problems of HgCdTe are believed to originate from vacancies; thus, understanding the causes for the high equilibrium vacancy density in this material is important to understanding the behavior of this alloy. In this paper, we present a theoretical model for the vacancy that not only gives good insight into the problem and lends itself naturally to an extension to alloys, but also yields reasonable estimates for the vacancy formation energies that can be compared with experiment. We have used a simple model to calculate the vacancy energies in all tetrahedral semiconductors based on Harrison's tight-binding theory.[5,6] We have modeled the vacancy and its immediate environment using a small cluster of atoms (out to the third shell) about the vacancy site. We consider two different final

states for the removed atom: (1) a quantity denoted the removal energy ΔE_r, is the energy to extract an atom from a bulk lattice site into a neutral, free-atomic final state and (2) the vacancy formation energy, $\Delta E_v(111)$, corresponds to a final state in which the atom ends on a (111) surface. The interactions of the cluster eigenstates with the extended crystal are included in second-order perturbation theory.[6] By including the interactions of the cluster with the extended crystal, we have in part eliminated the error introduced by describing the vacancy in a cluster calculation.

II. CLUSTER CALCULATIONS

A. *Removal energy*

First, we calculate ΔE_r, the energy necessary to remove an atom from the bulk crystal, and put it into a free-atomic final state. The initial and final states are both modeled by a cluster of atoms out to the third shell about the vacancy site, containing 104 and 100 hybrid orbitals respectively. The cluster Hamiltonian matrix elements are based on Harrison's tight-binding theory with universal scaling laws.[6] The site-diagonal matrix elements in the hybrid basis are

$$e_h^a = (e_s^a + 3e_p^a)/4 \quad \text{for an anion site,} \tag{1a}$$

and

$$e_h^c = (e_s^c + 3e_p^c)/4 \quad \text{for a cation site.} \tag{1b}$$

The matrix element coupling two hybrids on the same atom site are given by

$$V_1^a = (e_s^a - e_p^a)/4 \quad \text{for an anion site,} \tag{2a}$$

and

$$V_1^c = (e_s^c - e_p^c)/4 \quad \text{for a cation site.} \tag{2b}$$

Finally, the matrix element coupling two hybrids pointing toward one another is given by the hybrid covalent energy

$$V_2 = -3.22\ (\hbar/md^2). \tag{3}$$

After diagonalization of the cluster Hamiltonian, the cluster eigenstates are coupled to the bordering crystal bond-orbitals by second-order perturbation theory that corresponds to Harrison's metallization.[6] The metallization of the hybrids inside the cluster are explicitly included in the cluster diagonalization.

The removal energy is given by the difference between the initial- and final-state energies

$$\Delta E_r = E_f - E_i \tag{4}$$

where only energies that change upon the vacancy formation have been included. The initial-state cluster energy is given by

$$E_i = \sum_{i=1}^{N_h/2} 2(e_i + e_i^{met}) + \Delta E_{(out)}^{met} + 4\ V_0 \qquad (5)$$

where e_i are the eigenstates of the cluster Hamiltonian and i sums over the occupied states, and N_h is the number of electrons in the cluster; this equals the number of hybrids in the initial-state cluster. Here, e_i^{met} is the shift to the i^{th} cluster eigenstate caused by metallization with the crystal antibond orbitals at the cluster edges; ΔE_{out}^{met} is the energy shift of the bordering crystal bond orbitals from metallization, with the cluster antibonds coupling through an anion or cation at the cluster edge. V_0 is the repulsive energy between two hybrids in a bond and arises from the overlap of the hybrids and core states on adjacent sites. $4V_0$ is included in the initial-state energy for the four central bonds that are broken on creation of a vacancy. The average eigenstate energy of the cluster is used to determine the bond cohesive energy E_{ch}. Then, V_0 has been adjusted to yield cohesive energies in agreement with experiment.

The diagonalization of the final-state cluster yields a set of N_h-4 eigenstates. The lowest $(N_h-4)/2$ eigenstates correspond to the occupied cluster states, the highest $(N_h-4)/2$ eigenstates correspond to the unoccupied states, and the central four eigenstates correspond to the partially occupied dangling hybrid states that are largely localized on the four dangling hybrid orbitals pointing into the vacant site. Because we include out to the third shell of atoms about the vacancy site, the degeneracy of the four branches of atoms is split into one A_1 and three T_2 states. The energy of the final-state cluster is given by

$$E_f = \sum_{i=1}^{(N_h-4)/2} 2(e'_i + e'^{\,met}_i) + \sum_{i=[(N_h-4)/2]+1}^{[(N_h-4)/2]+1+N_d} (e'_i + e'^{\,met}_i) + \Delta E'^{met}_{out} + e_{atom} . \quad (6)$$

Here, N_d is the number of electrons in the four dangling hybrid states and is 2 (6) for an anion (cation) vacancy in a II-VI semiconductor. e_{atom} is the energy of the valence electrons of the removed atom in a free-atomic final state. All other terms are as defined for Eq. (5).

B. *Vacancy formation energy*

Removal energies should not be used as the energy parameters determining the vacancy concentrations or diffusion coefficients, although they give a good qualitative measure of structural integrity. A more appropriate energy to use is what we have termed the vacancy formation energy; it corresponds to the energy required to remove an atom from the bulk and put it on a free (111) surface where it can remake as many as three bonds. An accurate calculation requires a good knowledge of the surface reconstruction. We suggest a simple way to estimate the vacancy formation energy assuming only ideal surfaces.

Consider, for example, the II-VI crystal AB with nonreconstructed cation A and anion B surfaces with some A (B) sites available on the A (B) surface. The dangling hybrids on the B surface are either doubly or singly occupied, with an average of 1.5 electrons for each hybrid state. Similarly, half of the dangling hybrids on the cation A surface will have one electron, and half will have no electrons in them. Consider the removal of cation from the bulk; four bonds are broken and six electrons are left to occupy the dangling hybrids on the four surrounding anion hybrids. Each of the hybrids will be occupied by 1.5 electrons on average, which is similar to the B surface. The hybrids of the cation removed to a cation surface will be occupied by 0.5 electrons on average. Let the energy of the unit with three AB bonds connecting to a single A at a surface with an average of 0.5 electrons in the dangling bond be

E(A) (which includes only the back-bond and metallization energies), and similarly define E(B). Then, the vacancy formation energy for removal of a cation can be shown to be given by

$$\Delta E_v(\text{cation}) = [E(A) + E(B)] - E_b \tag{7}$$

$$= \frac{1}{8} [\Delta E_r(A) + \Delta E_r(B)]$$

where E_b is the energy per bond in the bulk.

One can show that the vacancy formation energy for the anion is also given by Eq. (7), using similar arguments. For both cation and anion, the vacancy formation energy is one-eighth of the average removal energy--roughly the energy to break just one bond. Because the most important mechanism in forming a vacancy is bond breaking, this result is not surprising. The difference between the cation and the anion vacancies will come from corrections to this energy caused by the Coulomb and rehybridization terms to be treated below.

C. *Corrections to* ΔE_v *and* ΔE_r

The cluster Hamiltonian does not include second neighbor interactions as it now stands; thus, the final-state dangling hybrids do not interact with one another. The inclusion of a dangling hybrid interaction results in an additional splitting of these states, with the A_1 level lowered by 3α, and the three T_2 levels each raised by an amount α. We assume that $\alpha = \alpha_{si}\ (\varepsilon_h/\varepsilon_h^{si})(d_{si}/d)^2$ where α_{si} is taken from Baraff, Kane, and Schlüter.[2]

Another contribution to the removal energy comes from the charge redistribution that occurs when a neutral atom is removed from the bulk of the crystal. When a neutral atom is extracted from the crystal, the charge previously residing on that site is redistributed about the vacancy. We estimate these charge shifts from projected local charge densities of the initial- and final-cluster eigenstates. Two contributions to the Coulomb energy are considered: the average electron-electron interaction energy, U when the electrons are on the same site, and the Madelung modified energy, K when one electron is on the anion and the other is on the cation.[7] Assuming all the charge redistribution is in the first shell of atoms about the vacancy site, the contribution to the vacancy energy that are caused by modifications in the electron-electron energy ΔU, is given by

$$\Delta U = \sum_i \frac{1}{2} U_i e^2 [(Z_i + \delta_i)^2 - (Z_i)^2] \tag{8}$$

$$= \left[-\frac{1}{2} U_0 - \frac{7}{8} U_1 \right] Z_0^2 e^2$$

where Z_0 is the net charge at the i^{th} atomic site and i sums over all atom shells, where i=0 is the central atom, i=1 is the first shell of 4 atoms, and so on. U_i differs from the cation to the anion site and are taken from van Schilfgaarde, Chen, and Sher.[7] δ_i is the charge modification at the i^{th} site with $\delta_0 = -Z_0$ and $\delta_i = (1/4)Z_0$, with all other charges unchanged. The changes in the Madelung energy also contribute to the vacancy formation energy by an amount given by

$$\Delta K = \sum_{i \neq j} \sum_{j} \frac{1}{2} \left[\frac{(Z_i + \delta_i)(Z_j + \delta_j)}{r_{ij}} - \frac{(Z_i)(Z_j)}{r_{ij}} \right] e^2 \qquad (9)$$

$$= \frac{31.2}{d} (Z_0)^2$$

where d is the bond length.

The removal energies will also be modified by Jahn-Teller distortion and lattice relaxation. These modifications have been calculated and found to be only a few percent and thus are neglected.

D. *Extension to dilute alloys*

The method is easily extended to alloys by explicitly replacing specific atoms within the cluster by a new species, because relatively small clusters of atoms have been used to describe the vacancies. For dilute cation-substituted alloys, the central cation in the cluster of some host lattice is replaced by a cation of the dilute species. The new cluster Hamiltonian is diagonalized and the cluster energy calculated as in Eq. (5); the final-state energy is that of a vacancy in the host lattice cluster plus the energy of a free cation of the dilute species. The removal energy is then calculated from Eq. (4). For the anion removal energies in a dilute cation substituted alloy, we consider how the anion removal energy will be modified when we replace one the of the cations adjacent to the removed anion by a cation of the dilute cation species. For nondilute alloys, we need to consider various classes of clusters with various distributions of cations of the two species. To calculate the alloy removal energy, the energy of each class of cluster must be weighted by the probability of its occurrence.

III. RESULTS AND DISCUSSION

Cation and anion removal energies were computed for ZnTe, CdTe and HgTe, and the results are listed in Table 1. Atomic term values were taken from Chen and Sher.[8] Modifications from Coulomb and rehybridization energies, and the corrected removal energies are also included. The removal energy for the anion is larger than for the cation for all compounds, as expected. For both cation and anion, removal energies for HgTe are smaller than those for ZnTe and CdTe; the removal energies are largest for ZnTe.

Removal energies were calculated for two cluster sizes: the large cluster of 104 hybrids in the initial state, and a smaller cluster containing 32 hybrid orbitals that is truncated at the second shell of atoms. For the II-VI compounds considered here, we found the removal energies changed by less than 18% for the cation, and less than 3% for the anion when we went from the small to the large cluster size. We will confirm the full convergence of this calculation in the future.

We have estimated the vacancy formation energies onto a (111) surface for HgTe, CdTe and ZnTe, using the removal energies computed above; the results are summarized in Table 2. Note that the vacancy formation energy is of order of the energy to break one bond compared to breaking four bonds for the removal energy. The difference between the removal and the vacancy formation energies is an estimate of the sublimation energy, ΔE_s from the (111) surface; values for ΔE_s are summarized in Table 2. The Hg is the easiest cation to evaporate from an A surface. For all compounds, Te is more difficult to remove from a B surface than the cations are to remove from an A surface. This large Te sublimation energy may be the reason for Te precipitates forming in HgCdTe.

We have, as a first approximation, calculated ΔE_r and $\Delta E_v(111)$ for dilute alloys only. Because the difference in both the removal and vacancy formation energies are small in Hg,

Cd and Zn, we linearly extrapolated the end points to obtain the concentrated alloy results. Results for $Hg_{1-x}Cd_xTe$ and $Hg_{1-x}Zn_xTe$ are shown in Fig. 1. The removal energies of Cd and Zn are always greater than that of Hg, and the anion Te is always the most difficult to remove. The cation energies are less sensitive to the alloy concentration x because the nearest neighbors to cations are always four Te anions.

We call the vacancy formation energy $\Delta E_v(111)$, and should emphasize that it refers to a very specific final state of a cation going to a (111) A surface, and an anion going to a (111) B surface. These final states correspond to the remaking of three bonds at the surface and, therefore, are the lowest energy unreconstructed surface-state possible. This final state necessarily implies that, for example, the (111) A face has several sites with cations missing with each of these sites serving as final states for the cation removed from the bulk. If no such sites are available, then one needs to consider the next lowest ΔE_v corresponding to the remaking of two bonds, e.g. on a (110) surface. Thus, we see that the vacancy formation energy is strongly dependent on *the final states available to the removed atom.* Because of this, it is difficult to make a direct comparison of our results with experimental data. In addition, the measured formation energies include contributions from interstitials as well as several possible charge states of the vacancy. Thus, a more extensive calculation needs to be completed before any reliable comparison with experiment can be done. However, we wish to note that these large differences in final states imply that diffusion coefficients measured on samples with a slab geometry will have thermal variations that are crystal-orientation dependent.

IV. SUMMARY AND CONCLUSION

In summary, we have calculated the ΔE_r, the energy to remove an atom from the bulk to a neutral free-atomic final state, and $\Delta E_v(111)$, the energy to remove a cation or anion from the bulk, and place it on the (111) A or B surface, thereby remaking three bonds. We have found Zn is the most difficult cation to remove from the II-VI compounds and alloys. This supports

the previous prediction based on the bond energies of HgTe in the Hg-based narrow gap II-VI alloys.[9] However, it is not sufficient to consider simply the bond energies when predicting vacancy formation energies. The creation of a vacancy involves not only the breaking of four bonds, but results in a back-bonding relaxation of the bonds about the vacancy site in the bulk, and this energy can be substantial. In addition, the formation of a vacancy results in rehybridization of dangling bonds and charge redistributions about the vacancy site. We find that dE_v/dx for Hg in HgCdTe is slightly positive, contrary to our earlier suggestion based only on bond energies.[9] However, dE_v/dx for Hg in HgZnTe is even larger, a trend in agreement with our prior predictions. In this first approximation, Hg vacancy formation energies in HgZnTe are always larger than those in HgCdTe, for concentrations producing band gaps in the range 0.1 to 0.3 eV. Therefore, by this measure, HgZnTe is the more stable material.

In conclusion, we find:

- $\Delta E_v^{Hg}(111)$ less in HgCdTe than in HgZnTe
- $\Delta E_v^{Te}(111)$ less in HgTe than in CdTe or ZnTe
- $\Delta E_v^{Te}(111)$ is surprisingly low
- Sublimation energy of Te large compared to Hg
- In slab geometry, ΔE_v is crystal-orientation dependent.

ACKNOWLEDGMENTS

This work was supported in part by NASA and NV&EOC Contract NAS1-12232, ONR Contract N00014-85-K-0448, and AFOSR Contract F49620-85-K-0023.

REFERENCES

1. S.G. Louie, M. #Schl{ u dotdot}ter#, J.R. Chelikowsky, and M.L. Cohen, Phys. Rev. B, 13, 1654 (1976).

2. G.A. Baraff, E.O. Kane, and M. #Schl{ u dotdot}ter#, Phys. Rev. B, *21*, 5668 (1980).

3. J. Bernholc, N.O. Lipari, S.T. Pantelides, Phys. Rev. B, *21*, 3545 (1980).

4. G.D. Watkins and R.P. Messmer, Phys. Rev. Lett., *25*, 656 (1970); Phys. Rev. B, *7*, 2568 (1973).

5. W.A. Harrison, *Electronic Structure and the Properties of Solids*, (Freeman, San Francisco, 1980).

6. W.A. Harrison, Microscience (limited distribution report, SRI International, Menlo Park, California) Vol. IV, p. 34 (1983).

7. M. van Schilfgaarde, A.-B. Chen, and A. Sher, Phys. Rev. Lett., *57*, 1149 (1986).

8. A.-B. Chen and A. Sher, Phys. Rev. B, *31*, 6490 (1985).

9. A. Sher, A.-B. Chen, W.E. Spicer, and C.K. Shih, J. Vac. Sci. Tech. A, *3*, 105 (1985).

TABLE I. Removal energies, ΔE_r, and corrections from rehybridization, ΔE_{ch}, $\Delta E(\alpha)$ and Coulomb energies $\Delta U + \Delta K$. Experimental cohesive energies are shown for comparison and were used in the determination of V_0. All energies are in units of eV.

Compound	E_{ch} (exp.)	ΔE_r		$\Delta E(\alpha)$		$\Delta U + \Delta K$		ΔE_r (corrected)	
		Cation	Anion	Cation	Anion	Cation	Anion	Cation	Anion
ZnTe	1.20	4.85	7.81	-0.41	-0.55	0.02	0.09	4.47	7.35
CdTe	1.10	4.40	6.98	-0.35	-0.48	0.05	0.21	4.10	6.71
HgTe	0.82	3.18	6.07	-0.35	-0.53	0.01	0.02	2.84	5.56

TABLE II. Vacancy formation energies, $\Delta E_v(111)$ for removal to a (111) surface and $\Delta E_s(111)$, the sublimation energy from a (111) surface, both in units of eV.

	$\Delta E_v(111)$ (corrected)		$\Delta E_s(111)$ (corrected)	
Compound	Cation	Anion	Cation	Anion
ZnTe	1.20	1.12	3.27	6.23
CdTe	1.12	1.15	2.98	5.56
HgTe	0.82	0.65	2.02	4.91

FIGURE CAPTION

Figure 1. Alloy variation of vacancy formation and removal energies in

(a) $Hg_{1-x}Cd_xTe$ *and*

(b) $Hg_{1-x}Z_xTe$

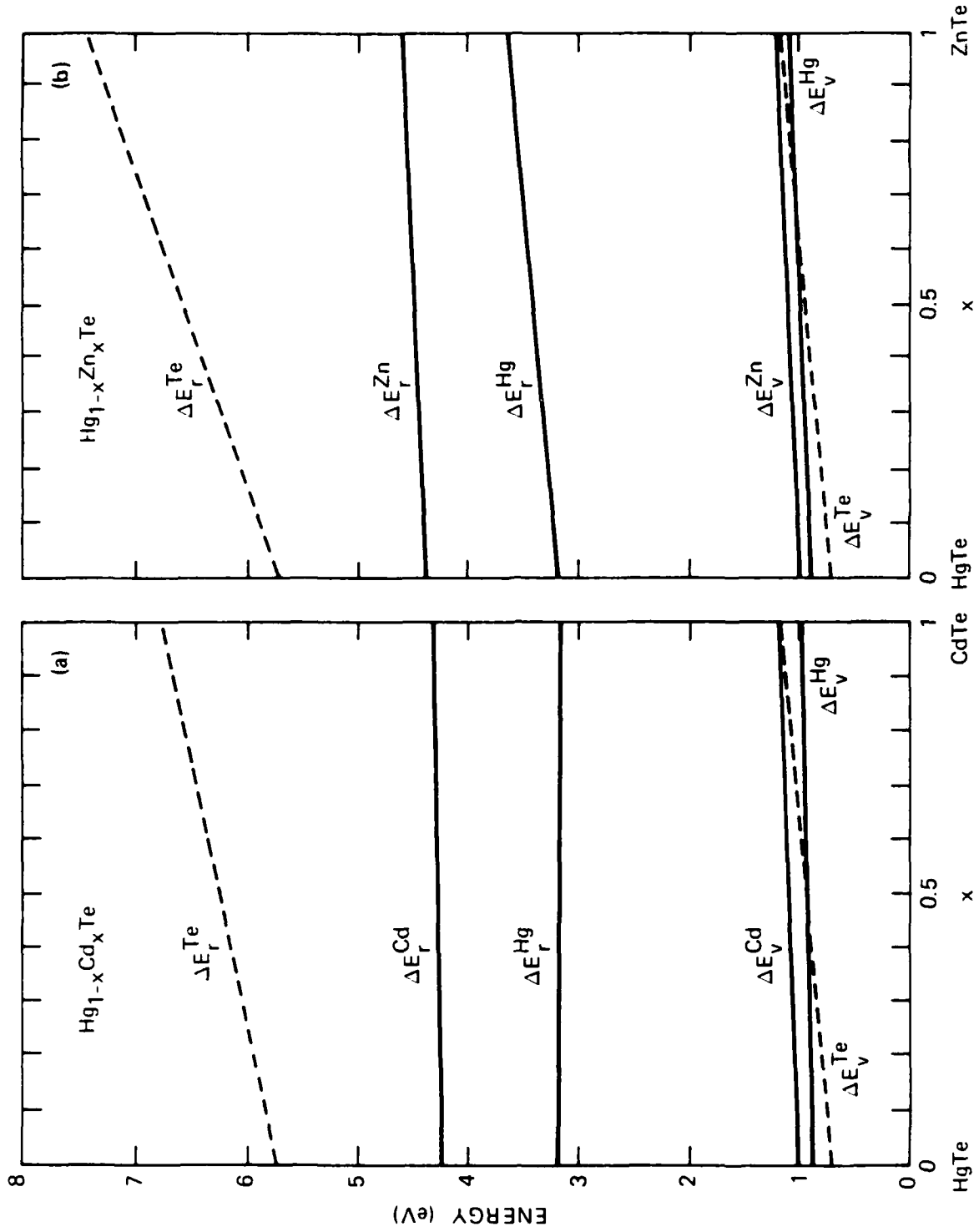

M. A. Berding, S. Krishnamurthy, A. Sher, A.-B. Chen
Fig. 1

Appendix C

CHRONOLOGICAL LIST OF PUBLICATIONS

Appendix C

CHRONOLOGICAL LIST OF PUBLICATIONS

1. A.-B. Chen, M. van Schilfgaarde, and A. Sher, "Formation Energies of Semiconductor Alloys: Dipolar Contributions," *Bull. Am. Phys. Soc.*, Vol. 31, p. 664 (1986).

2. M. van Schilfgaarde, A. Sher, and A.-B. Chen, "Atomic Correlations in Pseudobinary Semiconductor Alloys," *Bull. Am. Phys. Soc.*, Vol. 31, p. 664 (1986).

3. M. van Schilfgaarde, A.-B. Chen, and A. Sher, "Coulomb Energy in Pseudobinary Alloys," *Phys. Rev. Lett.*, Vol. 57, p. 1149 (1986).

4. A.-B. Chen, M.A. Berding, A. Sher, and M. van Schilfgaarde, "Vacancy Formation Energies in II-VI Semiconductors," The Workshop on the Physics and Chemistry of Mercury Cadmium Telluride (7-9 October 1986, Dallas, Texas).

5. A. Sher, A.-B. Chen and M. van Schilfgaarde, "Correlations in Pseudobinary Alloys," *J. Vac. Sci. Technol.*, Vol. A4, p. 1965 (1986).

6. A.-B. Chen, M. van Schilfgaarde, S. Krishnamurthy, M.A. Berding, and A.Sher, "Alloy Electronic Structure and Statistics," 7th Conference on Ternary and Multinary Compounds (10-12 September 1986, Snowmass, Colorado).

7. M. van Schilfgaarde, A.-B. Chen, and A. Sher, "Configuration Dependence of Coulomb Interactions in Pseudobinary Alloys," 7th Conference on Ternary and Multinary Compounds (10-12 September 1986, Snowmass, Colorado).

Appendix D

PARTICIPATING PROFESSIONAL PERSONNEL

Appendix D

PARTICIPATING PROFESSIONAL PERSONNEL

- M. Berding, Research Physicist, Physical Electronics Laboratory, SRI International
- A.-B. Chen, Professor, Auburn University, Auburn, Alabama
- S. Krishnamurthy, Research Physicist, Physical Electronics Laboratory, SRI International
- A. Sher, Staff Scientist, Physical Electronics Laboratory, SRI International
- M. van Schilfgaarde, Research Physicist, Physical Electronics Laboratory, SRI International

Appendix E

INTERACTIONS

Appendix E

INTERACTIONS

We have established good work relations with Professor D. Stevenson and Professor W.E. Spicer at Stanford, who are doing experiments related to our theory. We also work closely with the Santa Barbara Research Center research group headed by T.N. Casselman. A relationship is beginning with Professors Faurie and Raccah at the University of Illinois in Chicago.

END

3-87

DTIC